

Design and Synthesis of Bio-Inspired Hydrogen Bond Donating Ligands: Toward the Development of Oxidation Catalysts that Function in Supercritical Carbon Dioxide

by

Irine S. Saminathan
B.S. University of Peradeniya, Sri Lanka, 2002

Submitted to the Department of Chemistry and the Faculty of the Graduate School of the University of Kansas in partial fulfillment of the requirements for the degree of Master's of Science

Robert C. Dunn (Co-Chair)

Andrew S. Borovik (Co-Chair)

Cory Berkland

Date defended: 27 February 2007

The Thesis Committee for Irine S. Saminathan certifies
That this is the approved Version of the following thesis:

**Design and Synthesis of Bio-Inspired Hydrogen Bond
Donating Ligands: Toward the Development of
Oxidation Catalysts that Function in Supercritical
Carbon Dioxide**

Robert C. Dunn (Co-Chair)

Andrew S. Borovik (Co-Chair)

Cory Berkland

Date approved: _____

ABSTRACT

Hydrogen bonds (H-bonds) are the primary type of non-covalent interactions found in the active site of a metalloprotein. In addition to the metal-ligand covalent interactions, H-bonds influence reactive intermediates formed during reaction processes, and regulate the secondary coordination spheres around the metal ions.

The synthetic systems developed in the Borovik group utilize intramolecular H-bonds to help regulate chemistry of the metal complexes. New urea-based tripodal ligands with either long hydrocarbon chains or fluorinated phenyl rings have been prepared in order to increase the solubility of metal complexes in carbon dioxide based solvents. Reactions of a new tripodal ligand, tris[*N*-(*p*-pentafluorophenylureayl)-*N*-ethyl]amine, (H_61^{PF}) with Fe(II) salts was studied and a series of Fe(II) complexes with H_61^{PF} was developed by varying the amount of base equivalents used during synthesis.

The structural properties of the metal complexes indicate the presence of intramolecular H-bonds and some unusual molecular structures. The Fe(II) hydroxide complex isolate has an unique hexagonal (Fe-OH)₃ core in its crystal structure. Reactivity studies with dioxygen have also been carried out with the Fe(II)- H_61^{PF} complexes. Preliminary studies on these Fe(II) complexes indicate that they are capable of undergoing oxidation with dioxygen.

ACKNOWLEDGEMENTS

I would like to express my sincere thanks to all who walked along with me throughout my education and helped me to finish this difficult task successfully. Without their contribution, support for this work and confidence in me, this goal would have been a dream, never to come true.

My heartfelt appreciation goes to my advisor Prof. Andrew S. Borovik. I would have not achieved this task without his guidance and courage. The help and advice he gave me when he was at KU and from California was wonderful. He was supportive and understanding for the decisions I made and stood by me whenever I was exhausted and discouraged of work due to stress. I enjoyed Chemistry and working together with the Borovik research group. They helped me along the way to the end of my degree. I take this opportunity to thank them for teaching me to learn and understand research skills and encouraging me throughout my career as a graduate research assistant. Many thanks, of course, must go to my teachers during my undergraduate career at the University of Peradeniya, Sri Lanka, and my graduate career at the University of Kansas. They all enlightened me and showed the path to the new era of my life.

My mother and late father along with my sisters I will never forget since their love and affection has been invaluable. They have been supportive in every step of my life and I thank them for being there when ever I needed them. I am really happy to achieve this goal today. It was one of the ambitions of my loving father's. He always wanted to give us an educated and better life and I'm sure he would have been very pleased to see me in this position if he were alive today.

A big thank you goes to all my friends who were with me through all of my ups and downs. They stood by me through the painful moments I had when my father was passing away, when I started my life here at KU in a completely different country

with people with different lifestyles and they also were there to share the joyful memories I had during my stay at KU.

For all of you, THANK YOU!

TABLE OF CONTENTS

List of Figures	viii
List of Schemes	ix
List of Tables	ix
Chapter One: Introduction	1
Role of H-Bonds in the Active Site of Metalloproteins	2
Synthetic Models of Metalloproteins	4
Previous Work on Anionic-Base Tripodal Ligands	
(a) Amide Tripodal Ligands	9
(b) Urea-Based Tripodal Ligands	10
Mechanistic Aspects	13
Moving Towards Carbon Dioxide-Based Solvents	15
Overview of the Following Chapters	18
References	19
Chapter Two: Design of Multidendate Tripodal Ligands: Synthesis and Reactivity of Their Iron Complexes	
Introduction	24
Experimental	25
(a) Tris[(<i>N</i> -pentafluorophenylureayl)- <i>N</i> -ethyl]amine (H_61^{PF})	27
(b) Tris[(<i>N</i> -octylureayl)- <i>N</i> -ethyl]amine (H_61^{oct})	27
(c) $K_2[Fe^{II}(H_41^{PF})_2]$	28
(d) $K_3[Fe_2^{II}(H_31^{PF})_2(OAc)]$	29
(e) $K_3[Fe_3^{II}(H_31^{PF})_2(OH)_3]$	29
(f) Oxidation reactions of $K_2[Fe^{II}(H_41^{PF})_2]$	30
(g) Oxidation reactions of $K_3[Fe_2^{II}(H_31^{PF})_2(OAc)]$	31
Results and Discussion	

(a) Ligand design	33
(b) Synthesis of metal complexes	35
(c) Characterization of the monomer and dimer	37
(d) Vibrational Spectroscopy of the monomer and dimer	39
(e) Characterization of the trimer	39
(f) Oxidation Reactions of Metal Complexes	41
Summary	42
References	44

Chapter Three: Solid-State Molecular Structure of Iron(II) Complexes with Intramolecular H-Bonds

Introduction	47
Crystallographic Methods	
(a) $K_2[Fe^{II}(H_41^{PF})_2]$	47
(b) $K_3[Fe_2^{II}(H_31^{PF})_2(OAc)]$	49
(c) $K_3[Fe_3^{II}(H_31^{PF})_2(OH)_3]$	51
Results and Discussion	
(a) Empty Cavity Iron ^{II} Complex	53
(b) Iron ^{II} -Acetate Complex	58
(c) Iron ^{II} -Hydroxide Complex	63
Stacking Arrangements in Phenyl Rings	70
Conclusion	71
References	73

LIST OF FIGURES

Figure 1.1.	Active site of Cytochrome P-450.	3
Figure 1.2.A.	Collman's "picket fence" porphyrin complex.	5
Figure 1.2.B.	The "Picket Fence" concept.	6
Figure 1.3.	Berreau's model complex for active site of LADH.	7
Figure 1.4.	Six coordinate $[\text{Fe}^{\text{III}}(\text{tnpa})(\text{OH})(\text{PhCOO})]$ complex.	8
Figure 1.5.	Tripodal ligands with amide motif.	10
Figure 1.6.	Features of the H-bonding cavity of $\text{H}_3\text{1}^{\text{t-Bu}}$.	11
Figure 1.7.	Tripodal ligands used in preparation of metal complexes.	12
Figure 1.8.	Proposed mechanism for dioxygen activation.	14
Figure 1.9.	Design of new ligands	18
Figure 2.1.	New ligands for use in metal oxidation chemistry.	33
Figure 2.2.	Urea-based ligands used in previous studies.	35
Figure 2.3.	Expected geometry of metal complex after metallation.	37
Figure 2.4.	FTIR spectrum of $\text{K}_3[\text{Fe}_3^{\text{II}}(\text{H}_3\text{1}^{\text{PF}})_2(\text{OH})_3]$.	40
Figure 2.5.	EPR spectrum of $\text{K}_2[\text{Fe}^{\text{II}}(\text{H}_4\text{1}^{\text{PF}})_2]$.	41
Figure 3.1.	Structure of $\text{H}_6\text{1}^{\text{tBu}}$ and $[\text{Fe}^{\text{II}}\text{H}_3\text{1}^{\text{tBu}}]^-$.	56
Figure 3.2.	Molecular structure of $[\text{Fe}^{\text{II}}(\text{H}_4\text{1}^{\text{PF}})_2]^{2-}$.	57
Figure 3.3.	Molecular structure of $[\text{Fe}_2^{\text{II}}(\text{H}_3\text{1}^{\text{PF}})_2(\text{OAc})]^{3-}$.	60
Figure 3.4.	H-bonding network of $[\text{Fe}_2^{\text{II}}(\text{H}_3\text{1}^{\text{PF}})_2(\text{OAc})]^{3-}$.	60
Figure 3.5.	Molecular structure of $[\text{Fe}_3^{\text{II}}(\text{H}_3\text{1}^{\text{PF}})_2(\text{OH})_3]^{3-}$.	65
Figure 3.6.	Stick model of $[\text{Fe}_3^{\text{II}}(\text{H}_3\text{1}^{\text{PF}})_2(\text{OH})_3]^{3-}$.	66
Figure 3.7.	H-bonding network of $[\text{Fe}_3^{\text{II}}(\text{H}_3\text{1}^{\text{PF}})_2(\text{OH})_3]^{3-}$.	68
Figure 3.8.	Commonly observed aromatic-aromatic interactions.	70

LIST OF SCHEMES

Scheme 2.1. Synthetic route for H_61^{PF} .	34
Scheme 2.2. Synthesis of metal complex.	36
Scheme 2.3. Synthesis of metal complexes 1 and 2 .	38
Scheme 2.4. Synthesis of the trimer 3 .	40

LIST OF TABLES

Table 3.1. Crystallographic parameters for $K_2[Fe^{II}(H_41^{PF})_2]$.	54
Table 3.2. Selected bond distances and angles for $K_2[Fe^{II}(H_41^{PF})_2]$.	58
Table 3.3. Crystallographic parameters for $K_3[Fe_2^{II}(H_31^{PF})_2(OAc)]$.	59
Table 3.4. Bond distances and angles for $K_3[Fe_2^{II}(H_31^{PF})_2(OAc)]$.	61
Table 3.5. Crystallographic parameters for $K_3[Fe_3^{II}(H_31^{PF})_2(OH)_3]$.	64
Table 3.6. Bond distances and angles for $K_3[Fe_3^{II}(H_31^{PF})_2(OH)_3]$.	69

CHAPTER ONE

INTRODUCTION

Transition metal complexes have been widely used as catalysts in preparation of various organic compounds; these compounds can be prepared through metal mediated chemical transformations such as atom or group transfer reactions. In nature metalloproteins do such transformations to make new organic compounds from another one. The proper arrangement of ligands in metalloproteins and their influence to form non-covalent interactions could be accounted for their effectiveness and selectivity in chemical transformations. This inspired many researchers to prepare model compounds that can perform chemical transformations as effectively as metalloproteins.

The purpose of the research described in this thesis is to prepare metal complexes with new hydrogen bond donor ligands and investigate their reactivity with dioxygen. The new ligands are designed to increase the metal complex's solubility in different reaction media. The reaction medium of interest for this project was supercritical carbon dioxide (*scCO*₂) because it is a solvent without C-H bonds and it is cheap, abundant and environmentally benign. Utilizing the new ligands/metal complexes in *scCO*₂ will assist in understanding the chemical and physical properties of the reaction intermediates and products formed upon reactions with dioxygen and ultimately will advance research in metal mediated transformations. Oxidation of

small organic molecules could be achieved via the transfer of metal-bound oxo ligand to these species.

Role of H-Bonds in the Active Site of Metalloproteins

Metalloproteins perform a wide variety of functions in animal and plant physiology. When a transition metal/metals attached to the active site of a protein it is categorized as a metalloprotein. Several different metallo-proteins are found in nature; the most common are Cu(II), Co(II) and Fe(II)-containing proteins. Heme and non-heme Fe(II)-containing proteins are responsible for various functions in the human body such as oxygen transport, electron transport and storage. Transport of oxygen in mollusks and arthropods is controlled by the Cu(II)-containing metalloprotein hemocyanin.

A number of bonding and non-bonding interactions found around the metal ion(s) in the primary and secondary coordination sphere helps regulate the activity of a metalloprotein. Atoms or functional groups directly attached to the metal center define the primary coordination sphere, and the neighboring groups surrounding the primary sphere define the secondary coordination sphere of the metal. Even though the structure/function relationship of a metalloprotein relies mostly on the interactions found in primary coordination sphere, the non-bonding interactions (H-bonding, Lewis acid-base, electrostatic and hydrophobic-hydrophilic interactions) found in the secondary coordination sphere can also play an important role in controlling protein function. H-bonding interactions are the primary type of interactions. Many

metalloproteins show H-bonding interactions in their active sites and the structure and function of such proteins are often controlled by these interactions. The classic examples in which these interactions can be found are hemoglobin, myoglobin and cytochrome P450. Use of H-bonds in metal mediated atom transfer reactions and stabilization of intermediate/product formation is well illustrated in these proteins.

Cytochrome P450, a non-heme containing monooxygenase, catalyzes the activation of hydrocarbons in the presence of dioxygen and yields oxidative products.¹ The dioxygen activation mechanism was studied from structural and crystallographic evidences obtained for the reaction intermediates of this enzyme. Upon dioxygen binding to iron, H-bonds involving with the bonded O₂ and the Asp₂₅₁ residue via an active site water molecule were observed. An active site representation of cytochrome P450 is given in **Figure 1.1**.

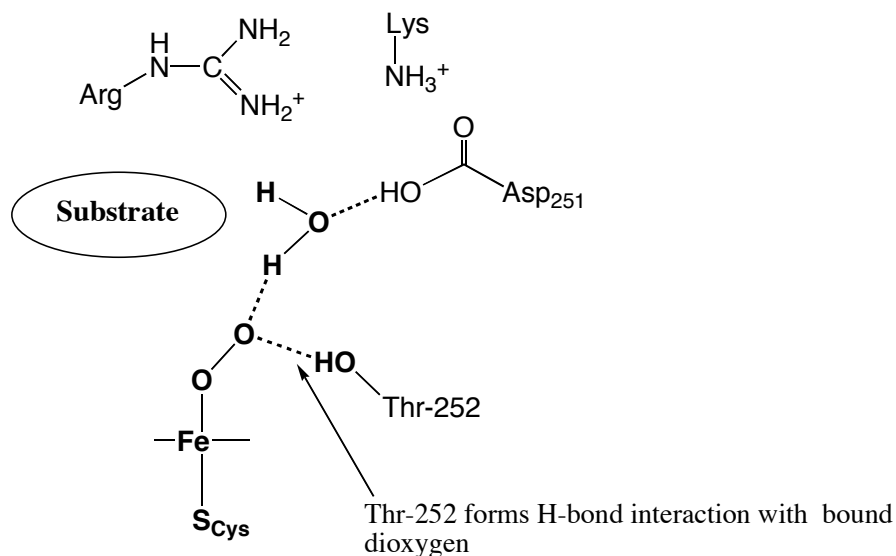


Figure 1.1. Active site of Cytochrome P-450. Dashed lines indicate H-bonding interactions.²

Studies indicate that the heterolytic O—O bond cleavage of the iron bound O₂, produces a high valent Fe(IV)=O(porphyrin radical) and a water molecule. The O—O bond cleavage requires proton transfer from the Thr-252 residue.² The hydroxyl group of this residue is found to be within the hydrogen bonding distance to the iron bound O₂. Replacing the hydroxyl group of Thr-252 shuts down the proton delivery mechanism and produces other products such as hydrogen peroxide.² Therefore it was concluded that the proper function and reactivity of cytochrome P450 relies on H-bonding interactions. Transfer of the iron-bound oxygen to substrates is also mediated by H-bonds.

Synthetic Models of Metalloproteins

Attempts have been made to mimic the secondary coordination sphere interactions found in the active sites of the metalloprotein synthetically, but without much success. When functional groups are placed within close proximity to the metal center they often form intermolecular H-bonding interactions with another functional group of the metal complex or with solvent molecules rather than forming intramolecular H-bonding interactions. To prevent this, H-bond donor/acceptor groups are incorporated into the synthetic molecule so that they can form a rigid framework and can facilitate intramolecular H-bonding interactions.

The “picket fence” porphyrin model complex synthesized by Collman and coworkers is one of the successful examples for metalloprotein synthetic models because the complex mimics the active sites found in heme proteins hemoglobin and

myoglobin (**Figure 1.2**).³ The pivalamide groups on the complex allows for the preferential coordination of small ligands/molecules to the active metal center and also prevent ligands undergoing further reactions with other functional groups.³ Because the “picket fence” architecture provides a protected pocket to the coordinated Fe-dioxygen adduct, further reactions of coordinated dioxygen with other iron-porphyrin complexes are avoided.⁴ Reversible dioxygen binding is observed in these porphyrin model complexes. However, no intramolecular H-bond interactions were observed between the H-bond donors in the pivalamide groups and the Fe—O—O moiety.

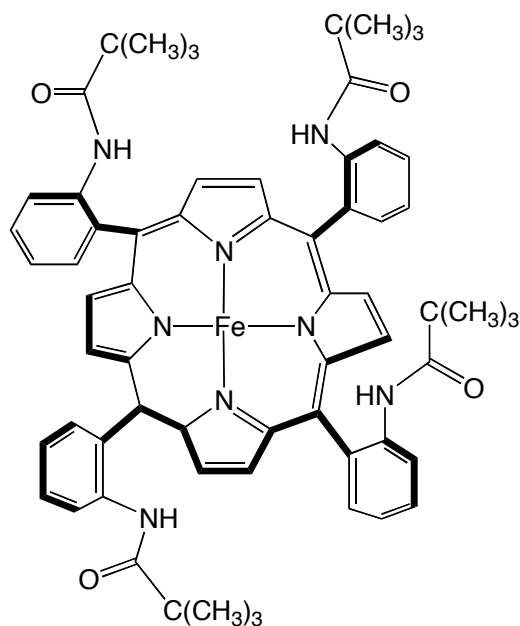


Figure 1.2. (A) Collman’s “picket fence” porphyrin complex.

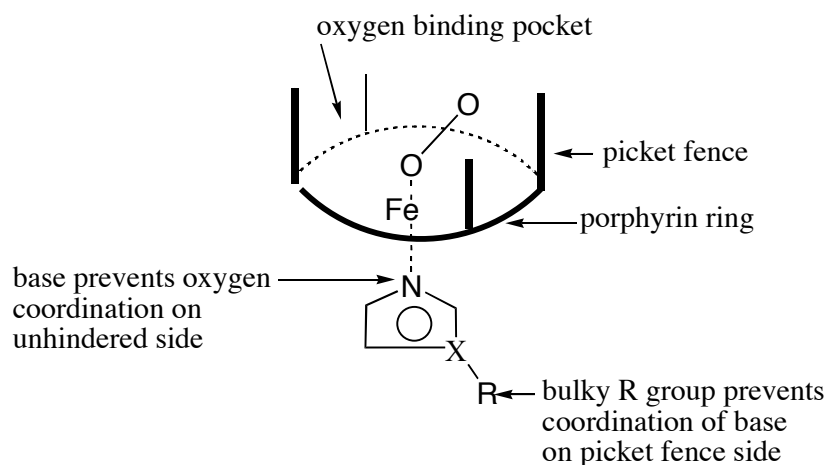


Figure 1.2. (B) The “Picket Fence” concept.⁴

Further research on this area by Reed⁵, Nocera⁶ and Chang⁷ led to the development of new porphyrin systems, in which H-bond donors have been attached to different substituents on the porphyrin ring to facilitate H-bonding interactions. Recently, Berreau has reported a new ligand [bmapa, *N,N*-bis-2-(methylthio)ethyl-*N*-(6-amino-2 pyridylmethyl)amine), where the coordination chemistry of this ligand with zinc ions mimics the active site of liver alcohol dehydrogenase(LADH) enzyme (**Figure 1.3**).⁸ In the body, this particular enzyme oxidizes alcohols to either aldehydes or ketones.⁹ A serine residue (Ser₄₈) in the active site of LADH corresponds to the intramolecular H-bonding interactions observed between the hydroxyl oxygen of Ser₄₈ and the zinc-bound alcohol proton.¹⁰ A single, strong intramolecular H-bonding interaction was observed in Berreau’s bmapa-zinc system when methanol or *N,N*-dimethylformamide was coordinated to the metal center.

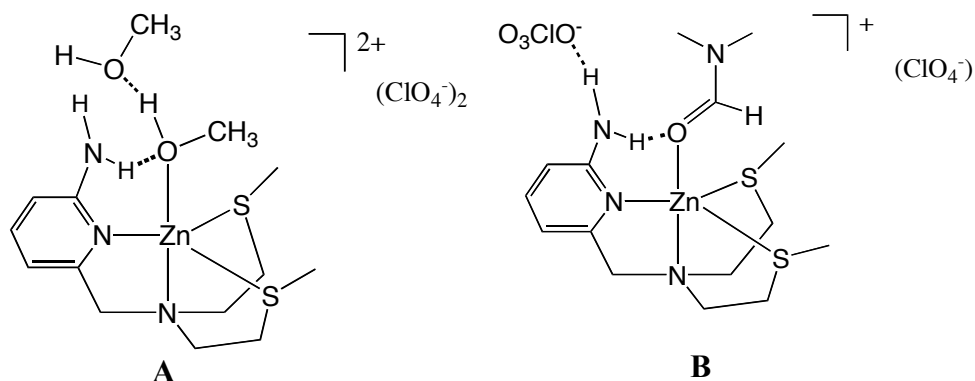


Figure 1.3. Representation of Berreau's model complex for the active site of LADH (A)-bmapa-Zn-MeOH complex (B)-bmapa-Zn-DMF complex

With the development of the tripodal ligand, bis(6-pivalamide-2-pyridylmethyl)(2-pyridylmethyl)amine (bppa) by Masuda and coworkers¹¹ characterization of a mononuclear $\text{Cu}^{\text{II}}\text{—OOH}^-$ species was achieved. Hydroperoxo-copper species were found to be the primary intermediates of copper enzyme catalyzed oxidation reactions. Since Cu-bound metalloproteins/enzymes are one of the most important systems in animal physiology, study of the model complexes that mimic the active site of copper proteins are of the utmost interest. Masuda's $\text{Cu}^{\text{II}}\text{—OOH}^-$ complex relies on H-bonds to stabilize the complex: intramolecular H-bonding interactions were observed between the peroxo oxygen atom and the two-amine H atoms.

Another synthetic complex reported by Masuda utilizes the tripodal ligand, tris(6-neopentylamino-2-pyridylmethyl)amine (tnpa) to mimic the active sites found in soybean lipoxygenase-1(SLO-1) enzyme. A six-coordinate Fe(III) center is proposed

in the catalytic cycle of the non-heme SLO-1. Intramolecular H-bonding interactions are also implicated in this enzyme involving the Fe(III)-OH₂ unit. Masuda's complex also has a six coordinate Fe(III) center, where the three pyridine nitrogens and the tertiary amine nitrogen of the tripodal ligand tnpa bind to the Fe(III) center in a tetradentate manner, leaving two open coordinate sites for hydroxo and carboxylato ligands.¹² **Figure 1.4** shows the structure of the ligand TNPA and the six-coordinate Fe(III) complex. Intramolecular H-bonding interactions are observed between the oxygen atom of the exogenous ligands and the NH's of the three-pyridine groups.

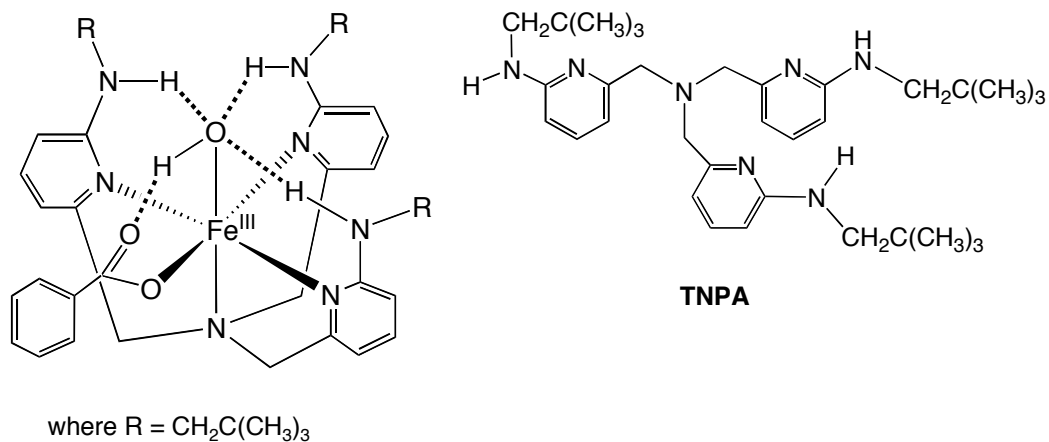


Figure 1.4. Six coordinate [Fe^{III}(tnpa)(OH)(PhCOO)] complex with intramolecular H-bonds.

Previous Work on Anionic-Based Tripodal Ligands

Development of tripodal ligands with suitable H-donor/acceptor groups has gained much interest in synthetic bioinorganic chemistry. H-donor/acceptor groups placed near the metal center that favors intramolecular H-bond formation with small molecules could be useful in regulating the reactivity of a synthetic metal complex.

Complexes designed within the Borovik group utilize key components of the molecular architectures found in the active site of metalloproteins. The research aim of the group is not only to develop model complexes that mimic the active site of a metalloprotein but also to study chemical transformations that utilize intramolecular H-bonds.¹³

(a) *Amide Tripodal Ligands*

Initial tripodal ligands developed within the group had deprotonated amide functional groups with different alkyl substituents. Some fundamental aspects of Collman's "Picket Fence" concept are taken in consideration to design these new ligands. They were designed to allow the ligation of small molecules to the vacant coordination site while providing a protecting cavity to prevent further bimolecular reactions. The amide tripodal ligands (**Figure 1.5**) enforce trigonal monopyramidal geometry when coordinated to a metal. Coordination of the external ligand to metal ion(s) is controlled by the nature of the substituents attached in the amides. It is possible to tune the microenvironment around the metal by varying these substituents. This leads to the formation of different metal complexes with various physical and chemical properties.¹⁴

An example of one system utilizing the tripodal ligand, tris(*N*-isopropylcarbamoylmethyl)amine¹⁴ is shown in **Figure 1.5B** illustrating how the reactivity of metal complexes can be varied by regulating the surrounding microenvironment. Formation of a paramagnetic Fe(II)—CO complex was achieved using this ligand.

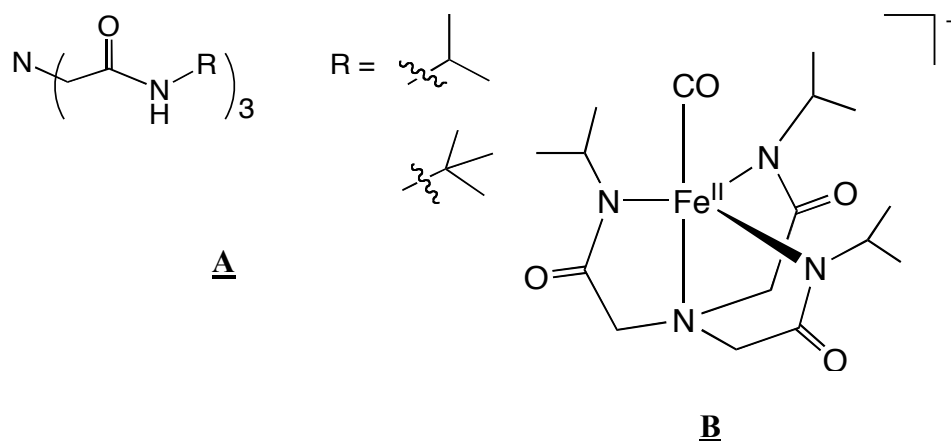


Figure 1.5. (A) Tripodal ligands with different substituents attached on the amide motif and (B) Fe(II)-CO complex with tripodal ligand, tris(*N*-isopropylcarbamoylmethyl)amine.

Complexes produced upon CO binding to Fe(II) center are usually diamagnetic; the observed paramagnetic complex formation is a result of the constrained microenvironment around the iron center caused by the ligand. The regulatory effect of the ligand is exemplified when tertiary butyl groups were substituted for the isopropyl substituents; binding of CO to the iron center was not observed in this case.

(b) Urea-Based Tripodal Ligands

Systems developed later in the group make use of deprotonated urea groups as the backbone of the ligand. Selection of urea groups is based on its ability to form H-bonds. The important structural features of complexes of the tripodal ligand, tris[(*N*'-tert-butylureayl)-*N*-ethylene]amine ($H_3\mathbf{1}^{t-Bu}$) are illustrated in **Figure 1.6**.¹³ The three *tert*-butyl urea groups radiate from an apical nitrogen atom, and are connected to the

apical nitrogen through three ethylene groups. Thus this urea-based ligand contains a three-fold symmetry axis.

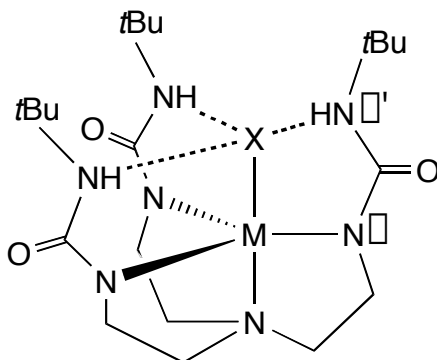


Figure 1.6. Features of the H-bonding cavity of H_31^{t-Bu} ligand. Dashed lines show intramolecular H-bonding interactions.

Each tripod arm contains two different NH groups denoted by □-NH, and □□NH. Deprotonation of the □-NH groups yields a trianionic ligand, which binds metal ions and forms three five-membered chelate rings. The remaining portions of the urea group serves as scaffolding for a rigid cavity surrounding to the metal center. The bulky *tert*-butyl groups on the ligand prevent unwanted metal-metal dimerization reactions. Three intramolecular H-bond interactions are observed between exogenous ligands ($X = O_2, OH^-, RNH_2$) and the three □□NH's, which are thermodynamically favored because six-membered rings are formed during H-bonding. Several other tripodal ligands have also been synthesized using urea groups as the backbone with different substituents (**Figure 1.7**). The above-mentioned features are also observed in all of these metal-ligand complexes.

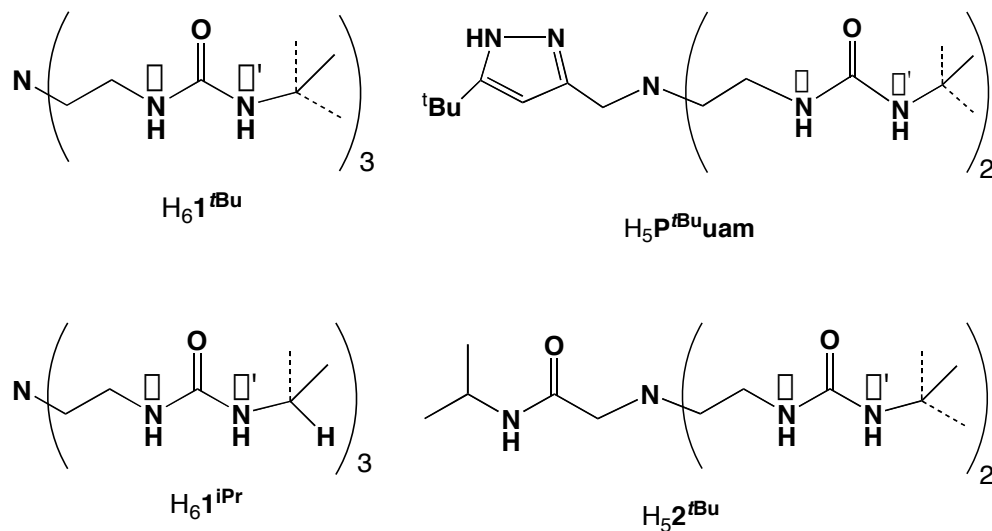


Figure 1.7. Tripodal ligands used in preparation of metal complexes.

The chemistry of these metal complexes was explored when they were treated for dioxygen activation. For example, activation of dioxygen was achieved when ligand H₃1^{t-Bu} was treated with four equivalence of base, and Fe(II) precursor and as a result stable monomeric iron-terminal oxo species [Fe^{III}H₃1^{t-Bu}(O)]²⁻ was isolated. An iron-terminal hydroxo species [Fe^{III}H₃1^{t-Bu}(OH)]⁻ was obtained from dioxygen activation when the ligand was allowed to react with three equivalence of base.¹⁵ Spectroscopic studies on the isolated dioxygen activated complexes [Fe^{III}H₃1^{t-Bu}(O)]²⁻ and [Fe^{III}H₃1^{t-Bu}(OH)]⁻ confirmed that the oxygen atom directly comes from the cleavage of dioxygen through labeling studies using ¹⁸O₂.

Several researchers have tried to isolate and characterize terminal iron-oxo complexes in the past. The terminal iron-oxo complex (Fe^{IV}=O) isolated by Que¹⁶ and

the stable ferrate ion, FeO_4^- by Hopper¹⁷ could be referred on this issue. However, dioxygen is not used as the source of oxygen for the formation of these complexes. Oxidants such as hydrogen peroxide or other oxygen-atom transfer reagents are used as the oxygen source instead. The Borovik group was the first to isolate the discrete iron coordination complexes with a terminal oxo ligand, which is derived directly from dioxygen. As a consequence of this, systems utilized to activate dioxygen within the Borovik group have drawn special attention in synthetic bioinorganic chemistry. It is worthwhile to mention that dioxygen activation is accomplished by the Fe(II) complexes of all the tripodal ligands that use urea groups.

Mechanistic Aspects

Figure 1.8 represents the proposed mechanism for dioxygen activation by an Fe(II) complex of ligand $\text{H}_3\mathbf{1}^{t\text{-Bu}}$. High valent metal-terminal oxo species ($\text{Fe}^{\text{IV}}=\text{O}$) are proposed to form during O_2 activation, which are immediately reduced to a metal-terminal hydroxo species ($\text{M}^{\text{III}}-\text{OH}$).¹⁵ The proposed explanation is that the $\text{Fe}^{\text{IV}}=\text{O}$ intermediate has a strong tendency towards H-atom abstraction; therefore as soon as it forms it abstracts a H-atom either from solvent molecules or an organic substrates present in the medium to produce the $\text{Fe}^{\text{III}}-\text{OH}$ species. Our mechanistic studies also indicate that “the $\text{M}^{\text{IV}}=\text{O}$ complexes have strong thermodynamic driving force to cleave C—H bonds with bond dissociation energies of less than 115 kcal/mol”.^{13, 18-19} Transfer of the oxo ligand to organic substrates is therefore hindered in these systems.

Because $M^{IV}=O$ species are the competent oxidant in these reactions, our group has interest in understanding their chemical and physical properties.

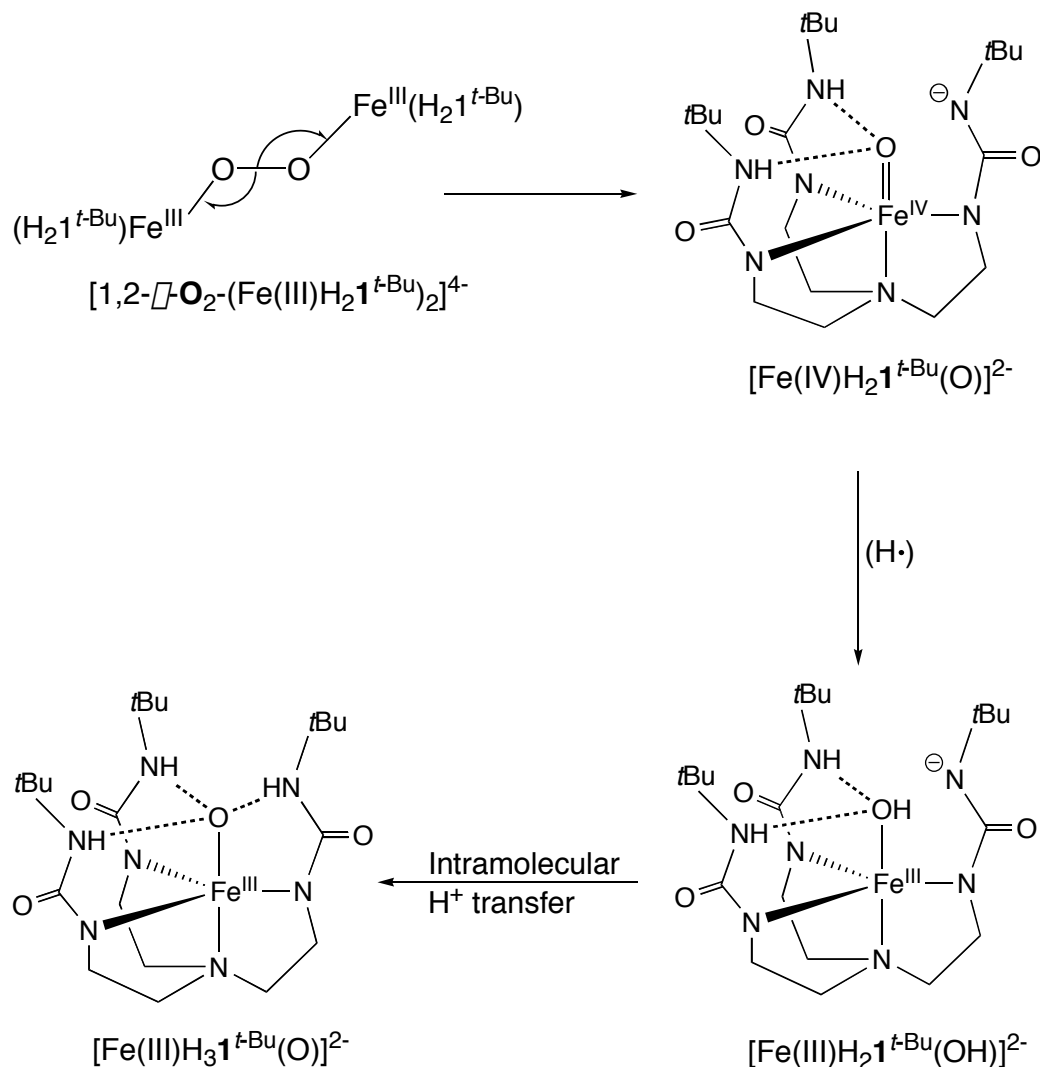


Figure 1.8. Proposed mechanism for dioxygen activation.¹⁵

In order to isolate and further enhance the reactivity of the high valent $M^{IV}=O$ intermediate ($M = Fe, Mn, Co$) reaction conditions need to be modified. Lowering

reaction temperature or changing reaction solvents can be applied to the system to capture this unstable species. For example, a stable monomeric $\text{Mn}^{\text{IV}}=\text{O}$ species was observed recently with ligand $\text{H}_3\mathbf{1}^{\text{t-Bu}}$ when the reaction temperature was lowered to $-45\text{ }^\circ\text{C}$ in dimethylformamide or at room temperature in dimethylsulfoxide (DMSO).²⁰ Transfer of the metal-bound oxo ligand from this oxomanganese species to some of the organic substrates was also achieved under those conditions. Because of this recent finding, it was believed that the utilization of different solvent media/temperature can be utilized to capture the transient $\text{M}^{\text{IV}}=\text{O}$ species in our studies.

Moving Towards Carbon Dioxide-Based Solvents

Changing the reaction medium from conventional organic solvents that have cleavable C—H bonds at room temperature and pressure to CO_2 -based media could eliminate hydrogen-atom abstraction from occurring. By using CO_2 -based media it is anticipated that the unstable $\text{M}^{\text{IV}}=\text{O}$ intermediates formed during the dioxygen activation can be identified and the metal bound oxygen atom can be efficiently transferred to organic substrates in CO_2 -based solvents. Supercritical CO_2 is chosen as a reaction medium for our studies.

Supercritical CO_2 ($sc\text{CO}_2$) offers many advantages as a solvent for many valuable chemical transformations and catalytic applications in chemical synthesis. Some of the beneficial factors are its low cost, low viscosity, nontoxic and nonflammable properties, moderate reaction conditions and its high availability and non-volatile

nature. A low critical temperature of 31.1°C and a low pressure of 7.38 MPa of *scCO*₂ make it more popular as a reaction medium.²¹

The chemical and environmental friendly nature of *scCO*₂ solvents would also be an added advantage. Using *scCO*₂ as a solvent would improve many industrially valuable chemical transformations because the miscibility of organic compounds and reactive gases (H₂, O₂) is greatly improved in this green solvent and thereby reducing mass-transfer limitations.²² Most importantly, *scCO*₂ significantly reduces environmental pollution because the emission of volatile organic compounds from *scCO*₂ is very low. Separation of the products formed during the reaction is more convenient and easier in *scCO*₂ than in neat conventional organic solvents. The aforementioned factors greatly enhance the productivity of chemical reactions in *scCO*₂. Also by varying the pressure and temperature of *scCO*₂, solubility of the reactants can be controlled. The change in solubility of the reactants and substrates can improve the activity and selectivity of such chemical reactions.

Because of all the important advantages of *scCO*₂ it was chosen as the solvent for the initial studies on **H₆1^{PF}** ligand. It was also expected that performing chemical reactions in *scCO*₂ would lead to the monitoring and analysis of dioxygen activation reactions under various pressure and temperature conditions. Often times the gas-liquid mixing (such as O₂ and the metal complex dissolved in an organic solvent) is the rate-limiting step in homogeneous catalytic reactions.²³ Such mixing would be more efficient in a single-phase system like *scCO*₂. Also found that in supercritical media concentrations of reactive gases were very much higher than in normal organic

solvents.²⁴⁻²⁵ Based on all these observations we anticipate that the activation of dioxygen by the metal complex could be more enhanced in *scCO*₂ than in normal organic solvents, and it would provide the opportunity to study the behavior of the reactive intermediates.

A concern with using *scCO*₂ solvents is the solubility of the metal complexes related with the early mentioned ligands. Because of the inadequate solubility of these metal-ligand complexes in *scCO*₂, the design of new ligands would be necessary. Literature survey on the concept of “solubility in *scCO*₂” reveals that when fluorinated groups/atoms are attached to a molecule, its solubility in *scCO*₂-based solvents increases substantially.²⁶⁻²⁹

Solubility data on phenyl 2,5-dichlorobenzenesulfonate (PDBS) and pentafluorophenyl 2,5-dichlorobenzenesulfonate (FPDBS) indicates that FPDBS dissolves more readily in *scCO*₂ than its non-fluorinated version. For example FPDBS dissolves in *scCO*₂ at 100 °C and 4750 psi, where as PDBS dissolves in *scCO*₂ at the same temperature but only at a pressure of 11,000 psi.³⁰ Because of this literature precedence, fluorinated derivatives of urea-based ligand systems should increase the solubility of the metal complexes. The research described herein involves with the design and development of fluorinated ligands and preparation of their iron complexes and their reactivity with dioxygen. Furthermore the development of ligands with long hydrocarbon chains is also part of the project. These teflon like ligands can also increase the metal complexes solubility in *scCO*₂. The new ligands developed are shown in **Figure 1.9**.

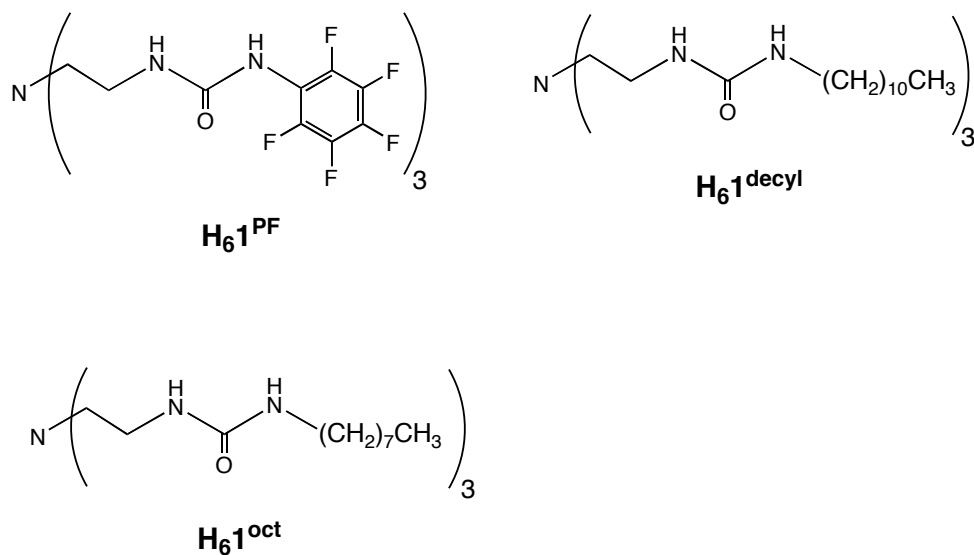


Figure 1.9. New ligands developed with fluorinated groups and long hydrocarbon chains.

Overview of the Following Chapters

Chapter 2 describes the preparation of the ligands and formation of several Fe(II) complexes. In addition, preliminary dioxygen reactions with these complexes are also discussed. Due to time constraints, the complete characterization of the reaction products that are obtained from dioxygen activation could not be achieved. Structural analysis of several of the Fe(II) complexes with the ligand tris[*N*-(2-pentafluorophenylureayl)-*N*-ethyl]amine (**H₆₁^{PF}**) is discussed in Chapter 3. Molecular structures of the three Fe(II) complexes and their unique binding features are included in this chapter.

References

1. Schlichting, I.; Berendzen, J.; Chu, K.; Stock, A. M.; Maves, S. A.; Benson, D. E.; Sweet, R. M.; Ringe, D.; Petsko, G. A.; Sligar, S. G. The Catalytic Pathway of Cytochrome P450cam at Atomic Resolution. *Science* **2000**, *287*, 1615-1622.
2. Gerber, N. C.; Sligar, S. G. Catalytic Mechanism of Cytochrome P-450: Evidence for a Distal Charge Relay. *J. Am. Chem. Soc.* **1992**, *114*, 8742-8743.
3. Collman, J. P.; Gagne, R. R.; Halbert, T. R.; Marchon, J.-C.; Reed, C. A. Reversible Oxygen Adduct Formation on Ferrous Complexes Derived from a “Picket Fence” Porphyrin. A Model for Oxymyoglobin. *J. Am. Chem. Soc.* **1973**, *95*, 7868-7870.
4. Collman, J. P.; Gagne, R. R.; Reed, C. A.; Halbert, T. R.; Lang, G.; Robinson, W. T. “Picket Fence Porphyrins.” Synthetic Models for Oxygen Binding Hemoproteins. *J. Am. Chem. Soc.* **1975**, *97*, 1427-1439.
5. Wuenschell, G. E.; Tetreau, C.; Lavalette, D.; Reed, C. A. H-Bonded Oxyhemoglobin Models with Substituted Picket-fence Porphyrins: The Model Compound Equivalent of Site-Directed Mutagenesis. *J. Am. Chem. Soc.* **1992**, *114*, 3346-3355.
6. Yeh, C.-Y.; Chang, C. J.; Nocera, D. G. “Hangman” Porphyrins for the Assembly of a Model Heme Water Channel. *J. Am. Chem. Soc.* **2001**, *123*, 1513-1514.

7. Chang, C. K.; Liang, Y.; Aviles, G. Conformational Control of Intramolecular Hydrogen Bonding in Heme Models: Maximal $\text{Co}^{\text{II}}\text{-O}_2$ Binding in a C-Clamp Porphyrin. *J. Am. Chem. Soc.* **1995**, *117*, 4191-4192.
8. Berreau, L. M.; Makowska-Grzyska, M. M.; Arif, A. M. Modeling the Active Site Chemistry of Liver Alcohol Dehydrogenase: Mononuclear Zinc Methanol and *N,N*-Dimethylformamide Complexes of a Nitrogen/Sulfur Ligand Possessing an Internal Hydrogen Bond Donor. *Inorg. Chem.* **2001**, *40*, 2212-2213.
9. Eklund, H.; Brändén, C.-I. In *Zinc Enzymes*; Spiro, T. G.; Ed.; Wiley: New York, 1983; pp 124-152.
10. Ramaswamy, S.; Eklund, H.; Plapp, B. V. *Biochemistry* **1994**, *33*, 5230-5237.
11. Wada, A.; Harata, M.; Hasegawa, K.; Jitsukawa, K.; Masuda, H.; Mukai, M.; Kitagawa, T.; Einaga, H. Structural and Spectroscopic Characterization of a Mononuclear Hydroperoxo-Copper(II) Complex with Tripodal Pyridylamine Ligands. *Angew. Chem. Int. Ed.* **1998**, *37*, 798-799.
12. Ogo, S.; Wada, S.; Watanabe, Y.; Iwase, M.; Wada, A.; Harata, M.; Jitsukawa, K.; Masuda, H.; Einaga, H. Synthesis, Structure, and Spectroscopic Properties of $[\text{Fe}^{\text{III}}(\text{tnpa})(\text{OH})(\text{PhCOO})]\text{ClO}_4$: A Model Complex for an Active Form of Soybean Lipoxygenase-1. *Angew. Chem. Int. Ed.* **1998**, *37*, 2102-2104.

13. Borovik, A. S. Bio-Inspired Hydrogen Bond Motifs in Ligand Design: The Role of Non-Covalent Interactions in Metal Ion Mediated Activation of Dioxygen. *Acc. Chem. Res.* **2005**, *38*, 54-61.
14. Ray, M.; Golombek, A. P.; Hendrich, M. P.; Young, Jr., V. G.; Borovik, A. S. Synthesis and Structure of a Trigonal Monopyramidal Fe(II) Complex and Its Paramagnetic Carbon Monoxide Derivative. *J. Am. Chem. Soc.* **1996**, *118*, 6084-6085.
15. MacBeth, C. E.; Golombeck, A. P.; Young, Jr., V. G.; Yang, C.; Kuczera, K.; Hendrich, M. P.; Borovik, A. S. O₂ Activation by Nonheme Iron Complexes: A Monomeric Fe(III)-Oxo Complex Derived From O₂. *Science* **2000**, *289*, 938-941.
16. Rohde, J.-U.; In, J.-H.; Lim, M. H.; Brennessel, W. W.; Bukowski, M. R.; Stubna, A.; Muenck, E.; Nam, W.; Que, L., Jr. Crystallographic and Spectroscopic Characterization of a Nonheme Fe(IV)=O Complex, *Science* **2003**, *299*, 1037-1039.
17. Hopper, M. L.; Schlemper, E. O.; Murmann, R. K. Structure of Dipotassium Ferrate(VI), *Acta Crystallogr.* **1982**, *B32*, 2237-2240.
18. Mayer, J. M. Hydrogen Atom Abstraction by Metal-Oxo Complexes: Understanding the Analogy with Organic Radical Reactions. *Acc. Chem. Res.* **1998**, *31*, 441-450.

19. Gupta, R.; Borovik, A. S. Monomeric Mn^{III/II} and Fe^{III/II} Complexes with Terminal Hydroxo and Oxo ligands: Probing Reactivity via O-H Bond Dissociation Energies. *J. Am. Chem. Soc.* **2003**, *125*, 13234-13242.
20. Parsell, T. H.; Behan, R. K.; Green, M. T.; Hendrich, M. P.; Borovik, A. S. Preparation and Properties of a Monomeric Mn^{IV}-Oxo Complex. *J. Am. Chem. Soc.* **2006**, *128*, 8728-8729.
21. Ballivet-Tkatchenko, D.; Camy, S.; Condoret, J. S.; Carbon dioxide, a Solvent and Synthone for Green Chemistry. *Environmental Chemistry* **2005**, 541-552.
22. (a) Pillai, U. R.; Sahle-Demessie, E.; Varma, R. S. Environmentally Friendlier Organic Transformations on Mineral Supports under Non-Traditional conditions. *J. Mat. Chem.* **2002**, *12*, 3199-3207. (b) Baiker, A. Supercritical Fluids in Heterogeneous Catalysis. *Chem. Rev.* **1999**, *99*, 453.
23. Rathke, J. W.; Klingler, R. J.; Krause, T. R. Propylene Hydroformylation in Supercritical Carbon Dioxide. *Organometallics* **1991**, *10*, 1350-1355.
24. Linke, W. F. Solubilities. *American Chemical Society: Washington, DC.* **1949**, *1*, 1077.
25. (a) Ungvary, F. J. *Organometal. Chem.* **1972**, *36*, 363-370. (b) Jessop, P. G.; Ikarlya, T.; Noyori, R. Homogeneous Catalytic Hydrogenation of Supercritical Carbon Dioxide. *Nature* **1994**, *368*, 231-233.
26. Eckert, Charles A.; Jessop, Philip G.; Liotta, Charles L. Solubilization and recovery of fluorinated compounds by adding and performing reactions with solvents and near-supercritical carbon dioxide. (The Regents of the University

- of California, USA; Georgia Tech Research Corporation). Application: WO, 2002, p 36 pp.
27. Wallen, Scott L.; Raveendran, P.; Blatchford, Marc A.; Schoenbachler, Laura K.; Chandrika, Baby; Dawson, Erica D. Novel CO₂-philes: Weak Hydrogen bonds, Solvation and Applications. In *Abstracts of Papers, 223rd ACS National Meeting*; Orlando, FL, 2002.
28. Elshani, S.; Du, H.; Laintz, K. E.; Natale, N. R.; Wai, C. M.; Elkarim, N. S. A.; Bartsch, R. A. Lariat Ether Carboxylic Acids, O-Benzylhydroxamates and Hydroxamic Acids with Fluorinated Substituents: Synthesis, Metal Ion Complexation and Solubility in Supercritical Carbon Dioxide. *Tetrahedron* **2000**, *56*, 4651-4657.
29. Mesiano, A. J.; Enick, R. M.; Beckman, E. J.; Russell, A. J. The phase behavior of fluorinated diols, divinyl adipate and a fluorinated polyester in supercritical carbon dioxide. *Fluid Phase Equilibria* **2001**, *178*, 169-177.
30. Wright, M. E.; Gorish, C. E.; Shen, Z.; McHugh, M. A. 2,5-Dichloro-1-(ROSO₂)benzene [R=C₆H₅, C₆F₅, and CH₂(CF₂)₄H]: Synthesis, Molecular Structure, and Solubility in Supercritical CO₂. *J. Fluorine. Chem.* **2006**, *127*, 330-336.

CHAPTER TWO

Design of Multidendate Tripodal Ligands: Synthesis and Reactivity of Their Iron Complexes

Introduction

The isolation and characterization of the high valent metal-terminal oxo species observed on our systems, are often limited by their high capability for abstracting hydrogen atoms from the solvent molecules or organic substrates present in the reaction medium. As a result of the abstraction process, metal-terminal hydroxo species are usually formed, which have been well studied and characterized in the past.¹ Replacing the normal organic solvents with solvents that do not have cleavable C-H bonds could eliminate H-atom abstraction by the metal complexes and help stabilize a terminal $M^{IV}=O$ species from the activation of dioxygen. Supercritical $CO_2(scCO_2)$ is the alternative solvent of interest because it does not have C-H bonds and it is environmentally benign.

Although the tripodal ligands and its metal complexes are soluble in traditional organic solvents their solubility is limited in $scCO_2$. Designing new organic ligands to improve the solubility of the metal complexes in supercritical CO_2 is crucial for any application. Synthesis of these new ligands followed procedures used in the past within the Borovik group² to make sure that the newer ligands have similar H-bonding properties.

Previous reports indicate that fluorinated functional groups enhance the solubility of organic compounds in supercritical CO₂.³⁻⁷ Therefore the new ligands were prepared either with long hydrocarbon chains or aromatic rings containing fluorine atoms. The preparation of these ligands is described in this chapter. In addition, the metal ion binding properties of the ligand tris[(*N*[2,3,4,5,6-pentafluorophenyl]ureayl)-*N*-ethyl]amine (**H₆1^{PF}**), which contains three fluorinated aromatic rings is further detailed in this chapter.

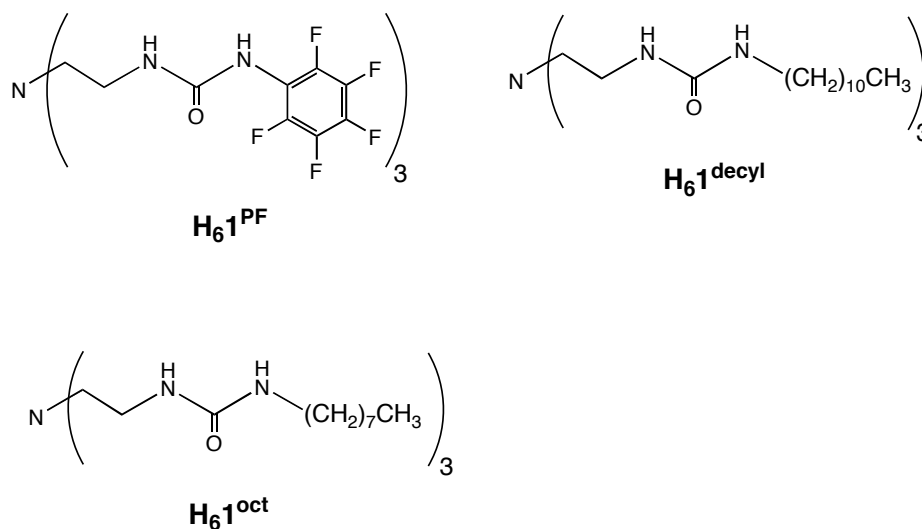


Figure 2.1. New ligands for use in metal oxidation chemistry.

Experimental

General Methods

Reagents used in all experiments were purchased from commercial sources and used as received. Anhydrous DMA was purchased from Aldrich and further

purified by eluting through a small silica-alumina column, and storing it under an inert atmosphere. All organic reactions were carried out under a N₂ atmosphere. Solid KH was prepared by washing the 30% potassium hydride dispersion in mineral oil, with pentane followed by Et₂O three times in a medium porosity glass frit and dried under vacuum and stored under an Ar atmosphere. All metal complexes were synthesized in a Vacuum Atmospheres, Co. drybox under an argon atmosphere. Dioxygen was dried on a Drierite gas purifier, which was purchased from Fisher Scientific. Elemental analysis of all the metal complexes was obtained from Desert Analytics (Tucson, AZ).

Physical Methods

Electronic spectra of the metal complexes were collected in a Cary 50 spectrophotometer using a 1.00 mm quartz cuvette. A Mattson Genesis series FT-IR instrument was used to record infrared spectra of the compounds and the spectral features are reported in wave numbers. ¹H NMR, ¹³C NMR, ¹⁹F NMR spectra were obtained with a Bruker Avance 400 MHz spectrometer. Perpendicular-mode X-band electron paramagnetic resonance (EPR) spectra were recorded using a Bruker EMX spectrometer equipped with an ER4102ST cavity and an ER041XG microwave bridge. Spectrometer settings for the EPR data collection were: attenuation, 25 dB; gain, 1.00 × 10³; conversion time, 81.920 ms; microwave frequency, 9.46 GHz; microwave power, 0.638 mW; modulation amplitude, 10.02 G; modulation

frequency, 100 kHz; sweep width, 5000 G; resolution, 1024 points and time constant, 655.36 ms.

Preparative Methods

Tris[(*N*-pentafluorophenylureayl)-*N*-ethyl]amine (H₆1^{PF}**):** A solution of tris(2-aminoethyl)amine (1.64 g, 11.2 mmol) in 81 mL of THF was cooled in an ice bath to 0°C. Pentafluorophenyl isocyanate (7.02 g, 33.6 mmol) was added drop wise to the solution with continuous stirring and a pinkish white precipitate was formed immediately. The reaction mixture was allowed to stir overnight under N₂ atmosphere at room temperature. The pink-white precipitate was filtered under suction, washed with diethyl ether, and dried to obtain a white fluffy solid. The product was dried under vacuum for 24 h to yield 6.91 g (80%) of a white solid. mp 189-192 °C; ¹H NMR (400 MHz, DMSO-*d*₆) δ 8.39 (3H, bs, *NHPh*), 6.59 (3H, t, *J* = 6 Hz, *NHCO*), 3.16 (6H, dt, *J* = 6 Hz, *NHCH*₂), 2.57 (6H, t, *J* = 6 Hz, *CH*₂*CH*₂); ¹³C NMR (500 MHz, CDCl₃) δ 154.96, 144.11, 142.20, 137.38, 115.18, 54.00, 40.13; FTIR (Nujol, cm⁻¹) 3331(*N*-H), 3281(*N*-H), 1646(urea C=O), 1003(s, Ph-F); Exact mass calcd for C₂₇H₁₉N₇F₁₅O₃ [*M*+*H*], 774.45. Found 774.13.

Tris[(*N*-octylureayl)-*N*-ethyl]amine (H₆1^{oct}**):** A solution of tris(2-aminoethyl)amine (1.00 g, 6.80 mmol) in 75 mL of THF was cooled in an ice bath to 0°C. Octyl isocyanate (3.40 g, 21.8 mmol) was added drop wise to the solution with continuous stirring. The reaction mixture was allowed to stir overnight under N₂ atmosphere at

room temperature. The white precipitate formed was filtered under suction, washed with diethyl ether, and dried under vacuum for 24 h to obtain 2.64 g (63%) of a white solid. ^1H NMR (400 MHz, CDCl_3) δ 6.19 (3H, t, $\text{NH}(\text{CH}_2)_7\text{CH}_3$), 5.71 (3H, t, NHCO), 3.15 (6H, dt, NHCH_2), 3.10 (6H, t, CH_2CH_2), 2.50 (6H, t, $\text{NHCH}_2(\text{CH}_2)_5$), 1.46 (6H, t, $(\text{CH}_2)_5\text{CH}_2\text{CH}_3$), 1.28 (30H, t, $(\text{CH}_2)_5\text{CH}_2\text{CH}_3$), 0.89 (9H, t, CH_2CH_3); ^{13}C NMR (500 MHz, CDCl_3) δ 159.70, 57.37, 55.48, 40.34, 31.89, 30.55, 29.52, 27.16, 22.68, 14.10; FTIR (Nujol, cm^{-1}) 3321(N-H), 3264(N-H), 1640(urea C=O); Exact mass calcd for $\text{C}_{33}\text{H}_{70}\text{N}_7\text{O}_3$ [M+H], 612.95. Found 612.55.

Potassium bis{[tris(*N*-pentafluorophenylureayl)-*N*-ethyl]aminato}ferrate(II)
 $\text{K}_2[\text{Fe}^{\text{II}}(\text{H}_4\text{1}^{\text{PF}})_2]$

To a solution of $\text{H}_6\text{1}^{\text{PF}}$ (100 mg, 0.13 mmol) dissolved in 3 mL of anhydrous DMA was added solid KH (10 mg, 0.26 mmol). The tan-yellow solution was allowed to stir for an hour until H_2 gas evolution had ceased. To this solution solid $\text{Fe}(\text{OAc})_2$ (12 mg, 0.065 mmol) was added and stirred for 30 min. The yellow mixture was filtered to remove insoluble KOAc (11 mg, 86%) and the filtrate was concentrated under reduced pressure to obtain a yellow solid. Then the yellow solid was washed with diethyl ether and dried under reduced pressure (110 mg, 50%). Vapor diffusion of Et_2O into a yellow solution of the product in DMA yielded single X-ray quality crystals. Anal. Calcd (found) for $\text{K}_2[\text{Fe}^{\text{II}}(\text{H}_4\text{1}^{\text{PF}})_2]$, $\text{C}_{54}\text{H}_{32}\text{FeK}_2\text{N}_{14}\text{F}_{30}\text{O}_6$: C, 39.20 (38.67); H, 2.50 (1.92); N, 11.69 (11.17); FTIR (Nujol, cm^{-1}) 3334(N-H), 3306(N-H), 1642(urea C=O), 1059(Ph-F), 992(s, Ph-F).

Potassium bis{[tris(*N*-pentafluorophenylureayl)-*N*-ethyl]aminato} (μ-acetato) K₃[Fe₂^{II}(H₃1^{PF})₂(OAc)]

To a solution of H₆1^{PF} (100 mg, 0.13 mmol) in 3 mL of anhydrous DMA solid KH (16 mg, 0.39 mmol) was added. The yellow-orange solution was allowed to stir for an hour until all H₂ gas evolution had ceased. To the solution solid Fe(OAc)₂ (23 mg, 0.13 mmol) was added and stirred for 30 min. The olive green mixture was filtered to remove insoluble KOAc (16 mg, 83%) and the filtrate was concentrated under reduced pressure to obtain a tan solid. The solid was washed with diethyl ether and dried under reduced pressure (123 mg, 52%). Vapor diffusion of Et₂O into a solution of the product in DMA yielded single X-ray quality crystals. Anal. Calcd (found) for K₃[Fe₂^{II}(H₃1^{PF})₂(OAc)], C₅₆H₃₃Fe₂K₃N₁₄F₃₀O₈: C, 37.37 (36.77); H, 2.36 (1.82); N, 10.52 (10.72); FTIR (Nujol, cm⁻¹) 3393(N-H), 3346(N-H), 1633(urea C=O), 1055(Ph-F), 997(s, Ph-F).

Potassium bis{[tris(*N*-pentafluorophenylureayl)-*N*-ethyl]amino}(tris-μ-hydroxo)triferrate(II) K₃[Fe₃^{II}(H₃1^{PF})₂(OH)₃]

To a solution of H₆1^{PF} (200 mg, 0.26 mmol) in 4 mL of anhydrous DMA solid KH (42 mg, 1.03 mmol) was added. The orange solution was allowed to stir until H₂ gas evolution ceased. Solid Fe(OAc)₂ (45 mg, 0.26 mmol) was added and stirred for 30 min. To the tan-brown mixture H₂O (4.7 mg, 0.26 mmol) was added and stirred for an hour. The reaction mixture turned to a light tan color while stirring, and KOAc was removed by filtration. The filtrate was concentrated under reduced pressure,

washed with diethyl ether and dried under reduced pressure to afford a tan solid (262 mg, 54 %). Vapor diffusion of Et₂O into a solution of the solid in DMA yielded X-ray quality crystals. FTIR (Nujol, cm⁻¹) 3629 (O-H), 3334(N-H), 1641(urea C=O), 1015(Ph-F), 996(s, Ph-F).

Oxidation reactions of potassium bis{[tris(*N*-pentafluorophenylureayl)-*N*-ethyl]aminato}ferrate(II) K₂[Fe^{II}(H₄1^{PF})₂]

Method A: To a solution of H₆1^{PF} (100 mg, 0.13 mmol) dissolved in 3 mL anhydrous DMA solid KH (10 mg, 0.26 mmol) was added. The tan-yellow solution was allowed to stir for an hour until H₂ gas evolution had ceased. Solid Fe(OAc)₂ (12 mg, 0.065 mmol) was added to the solution and stirred for 30 min. The yellow mixture was filtered to remove insoluble KOAc and the filtrate was concentrated under reduced pressure to obtain a yellow solid. The solid was washed with diethyl ether and dried under reduced pressure (107 mg, 49%). Dry dioxygen (1.6 mL, 0.065 mmol, 0.984 atm) was added via syringe to the DMA solution of the product obtained earlier (107 mg, 0.13 mmol). A dark red-orange solution formed upon the addition of dioxygen was allowed to stir for an hour, concentrated under reduced pressure and washed with diethyl ether to obtain a red solid (102 mg). FTIR (Nujol, cm⁻¹) 3357 (N-H); λ_{max} (DMA, nm) 382; X-band EPR (DMA, 77K) $g = 4.20$.

Method B: To a solution of H₆1^{PF} (100 mg, 0.13 mmol) dissolved in 3 mL anhydrous DMA solid KH (10 mg, 0.26 mmol) was added. The tan-yellow solution was allowed

to stir for an hour until H₂ gas evolution had ceased. Solid Fe(OAc)₂ (12 mg, 0.065 mmol) was added and stirred for 30 min. The yellow mixture was filtered to remove KOAc and the filtrate was concentrated under reduced pressure to obtain a yellow solid. The solid was washed with diethyl ether and dried under reduced pressure (107 mg, 49%). Me₃N□ O (10 mg, 0.13 mmol) was added to the DMA solution of the yellow product (107 mg, 0.13 mmol). The solution became dark red upon this addition and was stirred for an hour, concentrated under reduced pressure and washed with diethyl ether to obtain a red-brown solid (114 mg). FTIR (Nujol, cm⁻¹) 3357 (N-H); □_{max} (DMA, nm) 365; X-band EPR (DMA, 77K) g = 4.13.

Method C: The yellow solid K₂[Fe^{II}(H₄1^{PF})₂] (214 mg, 0.13 mmol) was dissolved in 4 mL anhydrous CH₃CN and anhydrous CH₂Cl₂ respectively. Addition of dry O₂ (1.6 mL, 0.065 mmol, 0.987 atm) or Me₃N□ O (10 mg, 0.13 mmol) to the dissolved K₂[Fe^{II}(H₄1^{PF})₂] produces a red solution, which was concentrated under reduced pressure and washed with diethyl ether to obtain a red solid. This red solid exhibits similar optical and EPR spectroscopic properties to the products prepared by method A and B.

Oxidation reactions of potassium bis{[tris(*N*-pentafluorophenylureayl)-*N*-ethyl]aminatoferrate(II)}(□-acetato) K₃[Fe^{II}(H₃1^{PF})₂(OAc)]

Method A: To a solution of H₆1^{PF} (100 mg, 0.13 mmol) in 3 mL anhydrous DMA solid KH (15 mg, 0.39 mmol) was added. The yellow solution was stirred an hour

until H₂ gas evolution ceased. To the solution solid Fe(OAc)₂ (23 mg, 0.13 mmol) was added and stirred for 30 min. The olive green mixture was filtered to remove insoluble KOAc and tetraethyl ammonium chloride (65 mg, 0.39 mmol) was added to the filtrate and stirred for 1 h. To the mixture Me₃N⁺ O⁻ (10 mg, 0.13 mmol) was added, and stirred for an additional hour. The dark red-brown solution was dried under reduced pressure to a red-brown solid and re-dissolved in anhydrous CH₃CN. Potassium chloride was removed via filtration through a fine frit and washed with diethyl ether, dried under reduced pressure and weighed (18 mg, 63%). The filtrate was concentrated under reduced pressure, washed with diethyl ether, dried to a brown solid (168 mg). FTIR (Nujol, cm⁻¹) 3264(N-H), 1697(urea C=O), 1055(Ph-F), 1001(s, Ph-F); ϵ_{max} (DMA, nm) 329s, 638b; X-band EPR (DMA, 77K) g = 4.15.

Method B: To a solution of H₆1^{PF} (100 mg, 0.13 mmol) in 3 mL anhydrous DMA solid KH (15 mg, 0.39 mmol) was added. The yellow solution was stirred an hour until H₂ gas evolution ceased. To the solution solid Fe(OAc)₂ (23 mg, 0.13 mmol) was added and stirred for 30 min. The olive green mixture was filtered to remove insoluble KOAc and tetraethyl ammonium chloride (65 mg, 0.39 mmol) was added to the filtrate and stirred for 1 h. To the mixture excess dry O₂ (0.984 atm) was added for 3 minutes, and stirred for an hour. The dark red solution was degassed and dried under reduced pressure to a red-brown solid and re-dissolved in CH₃CN. Potassium chloride was removed from the solution through filtration with a fine frit. The filtrate was concentrated under reduced pressure, washed with diethyl ether and dried under

reduced pressure to yield a brown solid (146 mg). FTIR (Nujol, cm^{-1}) 3216(N-H), 1697(urea C=O), 1055(Ph-F), 1001(s, Ph-F); λ_{max} (DMA, nm) 333; X-band EPR (DMA, 77K) $g = 4.15$.

Results and Discussion

Ligand design

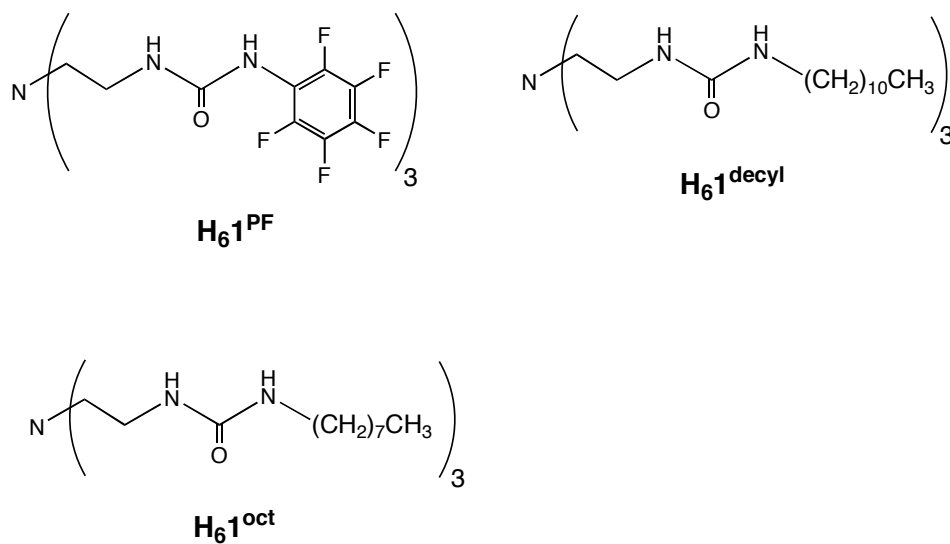
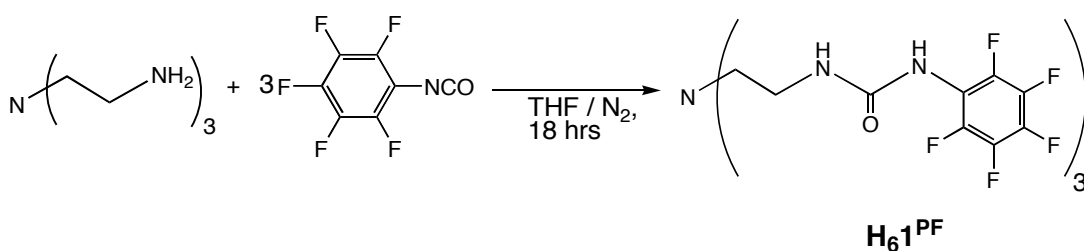


Figure 2.1. New ligands for use in metal oxidation chemistry.

Figure 2.1 shows the ligands developed in order to improve their metal complexes solubility in supercritical CO₂. All three ligands were prepared according to the procedure reported previously.² A free amine was coupled with the corresponding isocyanate in tetrahydrofuran under a dinitrogen atmosphere. The three-urea arms of the ligand are connected to a central nitrogen atom via three

ethylene spacers. Pentafluorophenyl isocyanate was allowed to react with tris(2-aminoethyl)amine in THF and the pinkish white precipitate formed was washed with diethyl ether and dried as H_61^{PF} with 86% yield. Likewise H_61^{oct} and H_61^{decyl} ligands were prepared by coupling tris(2-aminoethyl)amine with octyl isocyanate and decyl isocyanate, respectively. Because of the nature of long hydrocarbon chains in H_61^{oct} and H_61^{decyl} these ligands are isolated as oils.



Scheme 2.1. Synthetic route for H_61^{PF} .

The new ligand H_61^{PF} differs from the ligands prepared and used previously in the Borovik group because the three $\square\square NH$ protons are more acidic than the $\square-NH$ protons. The fluorinated phenyl ring makes the $\square\square NH$'s more acidic. Some examples of the ligands that have been prepared and used so far are given below (**Figure 2.2**).²

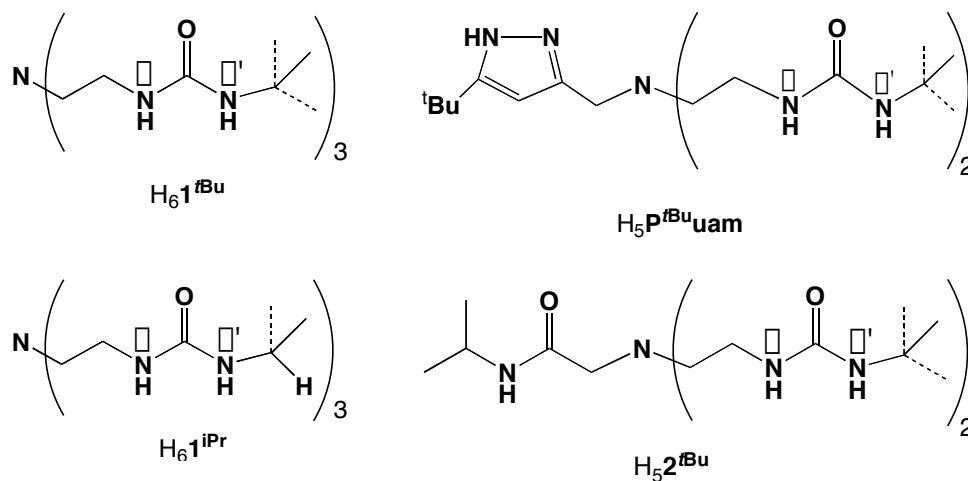
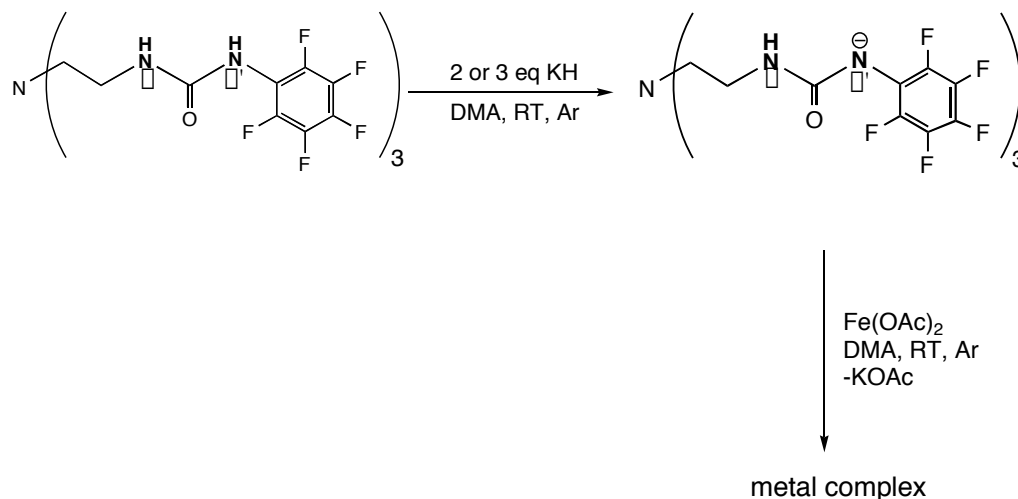


Figure 2.2. Urea-based ligands used in previous studies.

Synthesis of metal complexes

Upon the addition of base to H₆1^{PF} the □□NH protons are presumably deprotonated first producing a trianionic ligand (**Scheme 2.2**). The addition of metal salts to this trianionic species produces the metal complexes of interest. It was observed for ligand H₆1^{PF}; different metal complexes could be synthesized by varying the amount of base equivalents added to H₆1^{PF}.



Scheme 2.2. Synthesis of metal complex.

A trigonal monopyramidal geometry around the metal was expected upon coordination of the ligand $\text{H}_6\text{1}^{\text{PF}}$, because this structure is normally observed in complexes formed from similar ligands (**Figure 2.3**).² However, $\text{H}_6\text{1}^{\text{PF}}$ binds with Fe(II) ions to form a tetrahedral coordination sphere. Also when the number of equivalents of base varies, this ligand binds differently to the metal ion and produces complexes of different structures. However, in all cases the geometry around the metal was observed to be a tetrahedral. Details of the metal complex crystal structures and their specific features are discussed in Chapter 3.

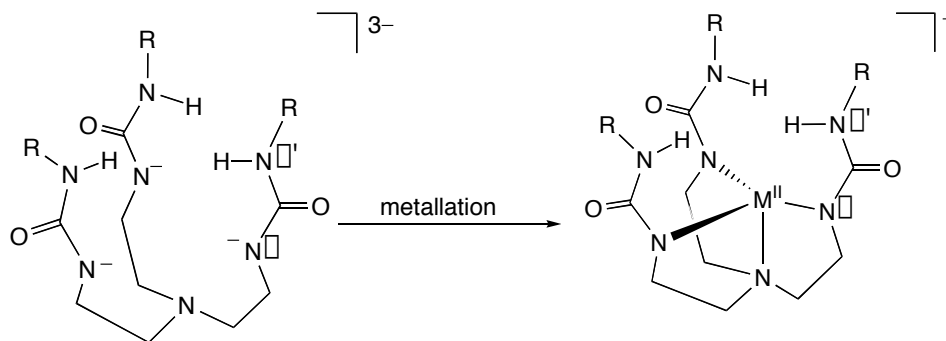
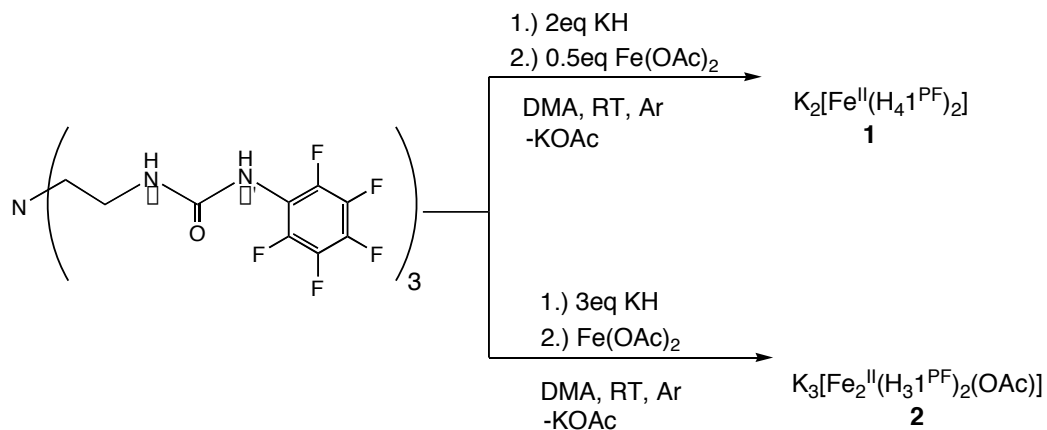


Figure 2.3. Expected geometry of the metal complex after metal binding.

Characterization of the monomer and dimer

The ligand H_61^{PF} produces a monomeric complex, $K_2[Fe^{II}(H_41^{PF})_2]$ (**1**) when it was treated with two equivalents of KH and half equivalent of iron acetate in anhydrous DMF under argon atmosphere. Complex **1** was soluble in DMA, DMF, CH_3CN and CH_2Cl_2 . One equivalent of KOAc was isolated from the reaction mixture as a white precipitate. In contrast, H_61^{PF} forms a dimer when it was treated with three equivalents of base and one equivalent of iron acetate to yield, $K_3[Fe_2^{II}(H_31^{PF})_2(OAc)]$ (**2**) and 1.5 equivalents of KOAc. Complex **2** was observed to be soluble in CH_3CN , CH_2Cl_2 and DMA. **Scheme 2.3** represents the formation of the two metal complexes.



Scheme 2.3. Synthesis of metal complexes **1** and **2**.

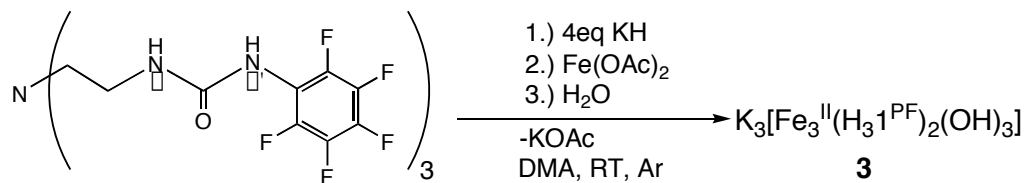
Single crystals were grown for the two complexes by dissolving each of them in a minimum amount of DMA and diffusing in diethyl ether. Complex **1** affords white single crystals while complex **2** produces yellow crystals. Crystal structures of the complexes were determined by X-ray diffraction studies. The yellow crystals were thin plates that are stacked together and the crystals are often twinned, which made the crystallographic analyses problematic. Even though these crystals were not well resolved (having an R value of 0.2856) the final structure obtained is both qualitatively and quantitatively definitive. Both complexes have a four coordinate geometry around the metal ion and two of the H₆1^{PF} ligands are present in the structure.

Vibrational Spectroscopic Analysis of the monomer and dimer

The Fourier transform infrared (FTIR) spectra collected for the monomer and dimer as Nujol mulls show distinct vibrational features. Both complexes show a broad N-H stretch in the region of 3300-3400 cm^{-1} , which indicates strong intramolecular H-bonding in the complexes.⁸ The $\text{H}_6\text{I}^{\text{PF}}$ ligand itself has two separate N-H stretches at 3282 cm^{-1} and 3337 cm^{-1} , which are absent in the spectra for the complexes. For the monomer, a sharp stretch was observed at 992 cm^{-1} and a small stretch at 1059 cm^{-1} , which are assigned to the $\square(\text{Ph-F})$ stretches. However, it differs from the free ligand where a sharp stretch was found at 1003 cm^{-1} , and a small stretch at 978 cm^{-1} . The change in peak shapes and energy may be considered as an indication of intramolecular H-bonding between the $\square\text{-NH}$ protons and the fluorine atoms in the aromatic ring. Likewise the dimer also exhibits a sharp vibration stretch at 997 cm^{-1} and a small stretch at 1055 cm^{-1} .

Characterization of the trimer

A trimeric complex, $\text{K}_3[\text{Fe}_3^{\text{II}}(\text{H}_3\text{I}^{\text{PF}})_2(\text{OH})_3]$ (**3**) formed when $\text{H}_6\text{I}^{\text{PF}}$ reacts with four equivalents of base, one equivalent of iron acetate and one equivalent of water (**Scheme 2.4**). The molecular structure obtained for the trimer also shows a tetrahedral geometry around the metal ion. However, the three Fe atoms are bridged through three hydroxyl groups, making a hexagonal unit inside the ligand cavity, with the cavity formed by two of the $\text{H}_6\text{I}^{\text{PF}}$ units.



Scheme 2.4. Synthesis of the trimer (**3**).

FTIR spectra collected on complex **3** confirm the presence of a hydroxo moiety in the complex. A weak FTIR band was observed at 3629 cm^{-1} (**Figure 2.4**), which is typical of a hydroxo vibration.⁹ Unfortunately, comparison of $\nu(\text{O-H})$ stretch of this $\text{Fe}^{\text{II}}\text{-OH}$ trimer with other $\text{M}^{\text{II}}\text{-OH}$ ($\text{M} = \text{Fe}, \text{Mn}, \text{Co}$) systems cannot be made at this point since the geometry of the trimer is different than any other $\text{M}^{\text{II}}\text{-OH}$ systems produced with the early ligands of the Borovik group.

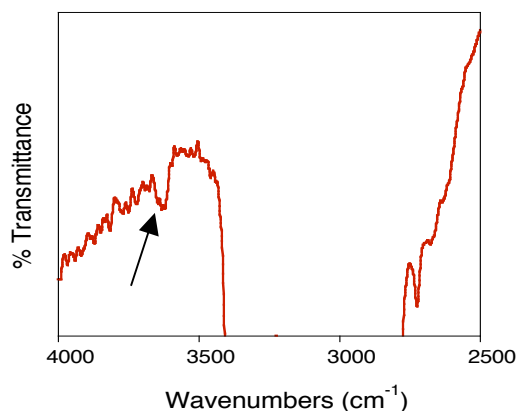


Figure 2.4. FTIR spectrum collected for $\text{K}_3[\text{Fe}_3^{\text{II}}(\text{H}_3\text{1}^{\text{PF}})_2(\text{OH})_3]$ in Nujol mull.

Oxidation Reactions of Metal Complexes

Addition of dry dioxygen to a solution of complex **1** in DMA produces a red-orange solution and a red solid was obtained when it was concentrated under reduced pressure. The EPR spectrum collected for the red solid is highly rhombic with a g value of 4.20, which is indicative of a $5/2$ -spin system. This confirms the formation of an Fe^{III} species in the reaction mixture. UV-vis spectrum of the red solid shows a new band at λ_{max} (DMA, nm) 382. This also suggests that the $\text{Fe}(\text{II})$ species is no longer present and it is oxidized in the system. However, the identity of the oxidative complex is still unknown; attempts to obtain a crystal structure for this species in different solvent systems were unsuccessful.

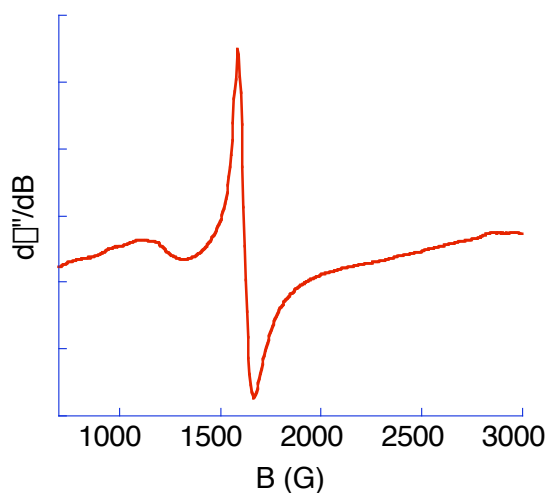


Figure 2.5. Perpendicular-mode X-band EPR spectrum collected for $\text{K}_2[\text{Fe}^{\text{II}}(\text{H}_4\text{1}^{\text{PF}})_2]$ in DMA after the addition of O_2 at 77K.

A similar kind of spectrum is observed for the red-brown solid obtained by method B, where one equivalent of $\text{Me}_3\text{N}\square\text{O}$ was added to complex **1** dissolved in DMA. Addition of $\text{Me}_3\text{N}\square\text{O}$ to complex **1** oxidizes the iron from a +2 oxidation state to +3 making it an EPR active species, which was confirmed by EPR spectroscopy. Unfortunately, methods followed to obtain a crystal structure of this complex were unsuccessful. However, predictions can be made that $\text{K}_2[\text{Fe}^{\text{II}}(\text{H}_4\text{I}^{\text{PF}})_2]$ is capable of being oxidizing, presumably by cleaving the O—O bond of dioxygen or the N—O bond of $\text{Me}_3\text{N}\square\text{O}$.

It was observed that complex **2** also undergoes oxidation under the same conditions followed for complex **1** and produces a brown solid. The EPR spectrum obtained for this solid has similar spectroscopic features that were shown in **Figure 2.5**. The UV-vis spectrum of the brown solid has a band at λ_{max} (DMA) 333 nm. Evidences obtained from the optical and EPR spectra of the brown solid suggest that the Fe(II) of the metal complex was oxidized when it treated with dioxygen. However, we were unsuccessful in completely solving the identity of these oxidized species.

Summary

New tripodal ligands were developed with hydrogen bond donating groups, and the solubility of such ligands was analyzed in different solvents. The ligands were designed to improve the metal complex's solubility in supercritical CO_2 . Derivatization of the early tripodal ligands with fluorinated groups makes this task

feasible. Reactions of the ligand H_61^{PF} with Fe(II) precursors were studied in detail under different reaction conditions. Three different Fe^{II} complexes were observed when ligand H_61^{PF} reacts with $Fe(OAc)_2$ under different deprotonating conditions. The oxidative properties of these complexes were studied and included in this chapter. Preliminary studies on the oxidized metal complexes confirmed that the addition of dioxygen can oxidize the Fe(II) center in both the monomer and dimeric complexes. Investigation on the oxidized Fe^{III} species of all metal complexes needs to be further explored. Even though the ligands/metal complex's were designed to function in supercritical CO_2 , preliminary dioxygen activation studies were carried out in traditional organic solvents and the chemistry of these metal complexes in supercritical CO_2 will be expected to investigate in near future.

References

1. MacBeth, C. E.; Golombeck, A. P.; Young, Jr., V. G.; Yang, C.; Kuczera, K.; Hendrich, M. P.; Borovik, A. S. O₂ Activation by Nonheme Iron Complexes: A Monomeric Fe(III)-Oxo Complex Derived From O₂. *Science* **2000**, *289*, 938-941.
2. (a) Borovik, A. S.; Hammes, Brian S.; Shirin, Z.; Yu, Qiang. Design of Hydrogen Bond Containing Cavities about Metal Ions. In *Book of Abstracts, 216th ACS National Meeting*, Boston, 1998. (b) Hammes, Brian S.; Young, V. G., Jr.; Borovik, A. S. Hydrogen-bonding Cavities about Metal Ions: A Redox Pair of Coordinatively Unsaturated Paramagnetic Co-OH Complexes. *Angew. Chem., Int. Ed.* **1999**, *38*, 666-669. (c) Lucas, R. L.; Powell, D. R.; Borovik, A. S. Development of Unsymmetrical Tripodal Ligands with Hydrogen Bond Motifs. (d) Lucas, R. L. Development of Hybrid Tripodal Ligands with Hydrogen Bond Motifs. Chapter 2, Dissertation, 2005.
3. Eckert, Charles A.; Jessop, Philip G.; Liotta, Charles L. Solubilization and recovery of fluorinated compounds by adding and performing reactions with solvents and near-supercritical carbon dioxide. (The Regents of the University of California, USA; Georgia Tech Research Corporation). Application: WO, 2002, p 36 pp.
4. Wallen, Scott L.; Raveendran, P.; Blatchford, Marc A.; Schoenbachler, Laura K.; Chandrika, Baby; Dawson, Erica D. Novel CO₂-philes: Weak Hydrogen

- bonds, Solvation and Applications. In *Abstracts of Papers, 223rd ACS National Meeting*; Orlando, FL, 2002.
5. Elshani, S.; Du, H.; Laintz, K. E.; Natale, N. R.; Wai, C. M.; Elkarim, N. S. A.; Bartsch, R. A. Lariat Ether Carboxylic Acids, O-Benzylhydroxamates and Hydroxamic Acids with Fluorinated Substituents: Synthesis, Metal Ion Complexation and Solubility in Supercritical Carbon Dioxide. *Tetrahedron* **2000**, *56*, 4651-4657.
 6. Mesiano, A. J.; Enick, R. M.; Beckman, E. J.; Russell, A. J. The phase behavior of fluorinated diols, divinyl adipate and a fluorinated polyester in supercritical carbon dioxide. *Fluid Phase Equilibria* **2001**, *178*, 169-177.
 7. Wright, M. E.; Gorish, C. E.; Shen, Z.; McHugh, M. A. 2,5-Dichloro-1-(ROSO₂)benzene [R=C₆H₅, C₆F₅, and CH₂(CF₂)₄H]: Synthesis, molecular structure, and solubility in supercritical CO₂. *J. Fluorine. Chem.* **2006**, *127*, 330-336.
 8. G. C. Pimentel and A. L. McClellan, *The Hydrogen Bond* (Freeman, San Francisco, 1960).
 9. (a) Shirin, Z.; Young, V. G., Jr.; Borovik, A. S. *Chem. Commun.* **1997**, 1967-1968. (b) Shirin, Z.; Hammes, B. S.; Young, V. G., Jr.; Borovik, A. S. Hydrogen Bonding in Metal Oxo Complexes: Synthesis and Structure of a Monomeric Manganese(III)-Oxo Complex and Its Hydroxo Analogue. *J. Am. Chem. Soc.* **2000**, *122*, 1836-1837. (c) MacBeth, C. E.; Golombeck, A. P.; Young, Jr., V. G.; Yang, C.; Kuczera, K.; Hendrich, M. P.; Borovik, A. S. O₂

Activation by Nonheme Iron Complexes: A Monomeric Fe(III)-Oxo Complex

Derived From O₂. *Science* **2000**, 289, 938-941.

CHAPTER THREE

Solid-State Molecular Structure of Iron(II) Complexes with Intramolecular H-Bonds

Introduction

Reactivity of the ligand H_6I^{PF} with iron salts, under different basic conditions was extensively studied and reported in the previous chapter. Several of the Fe(II)-complexes produced under different reaction conditions were crystallized via the vapor diffusion of diethyl ether in to a DMA solution of the complexes and the single crystals obtained were studied by X-ray crystallography. This chapter describes the structural details of three different metal complexes reported in chapter two.

Crystallographic Methods¹

$K_2[Fe^{II}(H_4I^{PF})_2]$

Colorless plate-shaped crystals of $K_2[Fe(C_{27}H_{16}F_{15}N_7O_3)_2] \cdot 4CH_3CON(CH_3)_2 \cdot 0.5O(C_2H_5)_2$ were selected for structural analysis. A full hemisphere of diffracted intensities (1850, 10-second frames with a scan width of 0.30°) was measured for a single-domain specimen using graphite-monochromated MoK- α radiation ($= 0.71073 \text{ \AA}$) on a Bruker SMART APEX CCD Single Crystal Diffraction System.² X-rays were provided by a fine-focus sealed x-ray tube operated at 50 kV and 35 mA. Lattice constants were determined with the Bruker SAINT software package using peak

centers for 5768 reflections. A total of 53217 integrated reflection intensities having $2\theta(\text{MoK}\alpha) < 61.09$ were produced using the Bruker program SAINT;³ 26088 of these were unique and gave $R_{\text{int}} = 0.040$ with a coverage which was 98.2% complete. The data were corrected empirically⁴ for variable absorption effects using equivalent reflections; the relative transmission factors ranged from 0.825 to 1.000. The Bruker software package SHELXTL was used to solve the structure using “direct methods” techniques. All stages of weighted full-matrix least-squares refinement were conducted using F_o^2 data with the SHELXTL Version 6.10 software package.⁵

The urea protons were located from a difference Fourier and initially included in the structural model as individual isotropic atoms whose parameters were allowed to vary in least-squares refinement cycles; they were then placed at idealized positions (assuming sp^2 -hybridization of the nitrogen atom and a N–H bond length of 0.88 Å). All methyl groups on the four crystallographically independent dimethylacetamide molecules and the disordered diethyl ether solvent molecule of crystallization were incorporated into the structural model as “staggered” rigid groups (using idealized sp^3 -hybridized geometry and a C–H bond length of 0.98 Å). The diethyl ether solvent molecule of crystallization is statistically (50/50) disordered with two orientations about the crystallographic inversion center at $(0, \frac{1}{2}, \frac{1}{2})$ in the unit cell. All additional hydrogen atoms were included into the structural model as idealized atoms (assuming sp^3 -hybridization of the carbon atoms and C–H bond lengths of 0.99 Å). The isotropic thermal parameters of all hydrogen atoms were fixed at values 1.2 (non-methyl) or 1.5 (methyl) times the equivalent isotropic thermal parameter of the

carbon or nitrogen atom to which they are covalently bonded.

The final structural model incorporated anisotropic thermal parameters for all non-hydrogen atoms and isotropic thermal parameters for all hydrogen atoms. A total of 1213 parameters were refined using no restraints, 26088 data and weights of $w = 1 / [(F^2) + (0.0854 P)^2]$, where $P = [F_o^2 + 2F_c^2] / 3$. Final agreement factors at convergence are: R_1 (unweighted, based on F) = 0.059 for 15672 independent absorption-corrected “observed” reflections having $2\theta(\text{MoK}\alpha) < 61.09$ and $I > 2(I)$; R_1 (unweighted, based on F) = 0.094 and wR_2 (weighted, based on F^2) = 0.165 for all 26088 independent absorption-corrected reflections having $2\theta(\text{MoK}\alpha) < 61.09$. The largest shift/s.u. was 0.001 in the final refinement cycle. The final difference Fourier had maxima and minima of $1.32 \text{ e}^-/\text{\AA}^3$ and $-0.65 \text{ e}^-/\text{\AA}^3$, respectively.

$\text{K}_3[\text{Fe}_2^{\text{II}}(\text{H}_3\text{I}^{\text{PF}})_2(\text{OAc})]$

Crystals of $\text{K}_2(\text{O}_2\text{CCH}_3)[\{\text{Fe}(\text{C}_{27}\text{H}_{15}\text{F}_{15}\text{N}_7\text{O}_3)\}_2(\text{O}_2\text{CCH}_3)] \cdot 4\text{CH}_3\text{CON}(\text{CH}_3)_2$ grown from dimethylacetamide and ether were selected for structural analysis. A full hemisphere of diffracted intensities (1850 50-second frames with an Δ scan width of 0.30°) was measured for a single-domain specimen using graphite-monochromated MoK- α radiation ($\lambda = 0.71073 \text{ \AA}$) on a Bruker SMART APEX CCD Single Crystal Diffraction System.² X-rays were provided by a fine-focus sealed x-ray tube operated at 50 kV and 30 mA. Lattice constants were determined with the Bruker SAINT software package using peak centers for 5167 reflections. A total of 26098 integrated reflection intensities having $2\theta((\text{MoK}\alpha)) < 39.56^\circ$ were produced using the Bruker

program SAINT;³ 9814 of these were unique and gave $R_{\text{int}} = 0.040$ with a coverage which was 99.9% complete. The intensity data were corrected empirically for variable absorption effects using equivalent reflections; the relative transmission factors ranged from 0.876 to 1.000. The Bruker software package SHELXTL Version 6.10⁵ was used to solve the structure using “direct methods” techniques. All stages of weighted full-matrix least-squares refinement were conducted using F_o^2 data with the SHELXTL software package.

The six crystallographically independent perfluorophenyl substituents were incorporated into the structural model as rigid groups (assuming a regular hexagonal of sp^2 -hybridized carbon atoms with C-C bond lengths of 1.39 Å and C-F bond lengths of 1.34 Å). Realistic metrical parameters could be obtained for most of the dimethylacetamide (and other) solvent molecules only when geometrical restraints were imposed. A free variable representing the length of a C-C single bond was included in the refinement to restrain selected segments of these disordered molecules. The bond lengths and angles for nonhydrogen atoms in ill-behaved solvent molecules were restrained to have values close to their idealized ones by requiring the separations between selected pairs of atoms to be near appropriate multiples the (C-C single-bond) free variable. This free variable refined to a final value of 1.447(2) Å.

The urea protons were included in the structural model at fixed idealized positions (assuming sp^2 -hybridization of the nitrogen atom and a N-H bond length of 0.88 Å). The remaining nonmethyl hydrogen atoms in the anionic metal complexes were included in the structural model as idealized atoms (assuming sp^3 -hybridization of the

carbon atom and a C-H bond length of 0.99 Å). Acetate methyl groups were incorporated into the structural model as rigid groups (using idealized sp³-hybridized geometry and a C-H bond length of 0.98 Å) with a “staggered” orientation. Hydrogen atoms were not included for solvent molecules. The isotropic thermal parameters of all hydrogen atoms were fixed at values 1.2 (nonmethyl) or 1.5 (methyl) times the equivalent isotropic thermal parameter of the nitrogen or carbon atom to which they are covalently bonded.

The final structural model incorporated anisotropic thermal parameters for the Fe and K atoms and isotropic thermal parameters for all other atoms included in the structural model.

K₃[Fe₃^{II}(H₃I^{PF})₂(OH)₃]

Colorless crystals of Na_{0.39}K_{2.61}[{Fe(OH)}₃(C₂₇H₁₅F₁₅N₇O₃)₂] \cdot 7.5 CH₃CON(CH₃)₂ \cdot 0.5 O(C₂H₅)₂ \cdot H₂O grown from dimethylacetamide and ether were selected for structural analysis. A full hemisphere of diffracted intensities (1850 40-second frames with an ω scan width of 0.30°) was measured for a single-domain specimen using graphite-monochromated MoK- α radiation (λ = 0.71073 Å) on a Bruker SMART APEX CCD Single Crystal Diffraction System.² X-rays were provided by a fine-focus sealed x-ray tube operated at 50 kV and 30 mA. Lattice constants were determined with the Bruker SAINT software package using peak centers for 9845 reflections. A total of 73687 integrated reflection intensities having $2\theta((\text{MoK}\alpha)) < 43.93^\circ$ were produced using the Bruker program SAINT;³ 28925 of these were unique

and gave $R_{\text{int}} = 0.056$ with a coverage which was 99.9% complete. The intensity data were corrected empirically for variable absorption effects using equivalent reflections; the relative transmission factors ranged from 0.918 to 1.000. The Bruker software package SHELXTL Version 6.10⁵ was used to solve the structure using “direct methods” techniques. All stages of weighted full-matrix least-squares refinement were conducted using F_o^2 data with the SHELXTL software package.

The benzene rings of the twelve crystallographically independent perfluorophenyl substituents were incorporated into the structural model as rigid groups (assuming a regular hexagonal of sp^2 -hybridized carbon atoms and a C-C bond length of 1.39 Å). Realistic metrical parameters could be obtained for most of the solvent molecules only when geometrical restraints were imposed. A free variable representing the length of a C-C single bond was included in the refinement to restrain selected segments of these disordered molecules. The bond lengths and angles for nonhydrogen atoms in ill-behaved solvent molecules were restrained to have values close to their idealized ones by requiring the separations between selected pairs of atoms to be near appropriate multiples the (C-C single-bond) free variable. This free variable refined to a final value of 1.437(2) Å.

The urea protons were included in the structural model at fixed idealized positions (assuming sp^2 -hybridization of the nitrogen atom and a N-H bond length of 0.88 Å). The remaining hydrogen atoms in the trianionic metal complexes were included in the structural model as idealized atoms (assuming sp^3 -hybridization of the carbon atom and a C-H bond length of 0.99 Å). Hydrogen atoms were not included for solvent

molecules. The isotropic thermal parameters of all hydrogen atoms were fixed at values 1.2 times the equivalent isotropic thermal parameter of the nitrogen or carbon atom to which they are covalently bonded.

The final structural model incorporated anisotropic thermal parameters for all cations and nonhydrogen atoms of the trianionic complex. Isotropic thermal parameters were incorporated for all included hydrogen atoms and all solvent nonhydrogen atoms. A total of 2305 parameters were refined using 178 restraints, 28925 data and weights of $w = 1 / [\sigma^2(F^2) + (0.2000 P)^2]$ where $P = [F_o^2 + 2F_c^2] / 3$. Final agreement factors at convergence are:

R_1 (unweighted, based on F) = 0.110 for 13872 independent absorption-corrected reflections having $2\theta(\text{MoK}\alpha) < 43.93^\circ$ and $I > 2\sigma(I)$; R_1 (unweighted, based on F) = 0.171 and wR_2 (weighted, based on F^2) = 0.348 for all 28925 independent absorption-corrected reflections having $2\theta(\text{MoK}\alpha) < 43.93^\circ$. The final difference map had maxima and minima of 1.30 and $-0.60 \text{ e}^-/\text{\AA}^3$, respectively.

Results and Discussion

Molecular Structure Results for the Empty Cavity Iron^{II} Complex

Single crystal X-ray diffraction studies were performed on $\text{K}_2[\text{Fe}^{\text{II}}(\text{H}_4\text{L}^{\text{PF}})_2]$ and the crystallographic parameters are given in **Table 3.1**. The asymmetric unit of $\text{K}_2[\text{Fe}(\text{C}_{27}\text{H}_{16}\text{F}_{15}\text{N}_7\text{O}_3)_2] \cdot 4\text{CH}_3\text{CON}(\text{CH}_3)_2 \cdot 0.5\text{O}(\text{C}_2\text{H}_5)_2$ contains two K^+ cations, one

[Fe(C₂₇H₁₆F₁₅N₇O₃)₂]²⁻ dianion or [Fe^{II}(H₄1^{PF})₂]²⁻, four dimethylacteamide molecules and half of a disordered diethyl ether solvent molecule of crystallization. The crystals have a triclinic, space group $P\bar{1}-C_1^1$ (No.2).⁶ Selected bond angles and distances are given in **Table 3.2**. The molecular structure of K₂ [Fe^{II} (H₄1^{PF})₂] is shown in Figure 3.2. All displacement ellipsoids are drawn at the 50% probability level.

Table 3.1 Crystallographic parameters for K₂[Fe^{II}(H₄1^{PF})₂].

Salt	K ₂ [Fe ^{II} (H ₄ 1 ^{PF}) ₂]
Empirical formula	C ₇₂ H ₇₃ F ₃₀ Fe K ₂ N ₁₈ O _{10.50}
Formula weight (g/mol)	2062.53
T (K)	100(2)
Space group	$P\bar{1}$
a (Å)	14.921(1)
b (Å)	17.583(1)
c (Å)	18.317(2)
α (deg)	95.659(2)
β (deg)	113.716(2)
γ (deg)	95.013(2)
Z	2
V (Å ³)	4335.3(6)
ρ _{calc} (Mg/m ³)	1.58
R ^a	0.059
R _w ^b	0.165
GOF ^c	0.956

^aR = $\frac{\sum |F_o|}{\sum |F_c|}$. ^bR_w = $\left\{ \frac{\sum [w(F_o^2 - F_c^2)^2]}{\sum [w(F_o^2)^2]} \right\}^{1/2}$. ^cgoodness of fit on F².

A unique feature is observed in all of the three Fe(II) complexes when ligand H_61^{PF} binds with iron salts. The metal ion forms coordinative bonds with the π -nitrogen atoms of the ligand rather than with σ -nitrogen atoms. Having pentafluorophenyl rings in the ligand makes the π -NH's more acidic than the σ -nitrogen protons; treating the ligand with base results in deprotonation of the π -NH groups. This explains the difference in ligand-metal binding between the H_61^{PF} ligand and all the other urea-based ligands used within the Borovik group. Once the ligand binds to the metal ion via π -nitrogen atoms, it arranges the coordination geometry to tetrahedral and leaves three σ -NH groups within the structure that are capable of forming intramolecular H-bonds with other atoms presence in close proximal. A similar pattern is also observed with the other urea-based ligands; however in such case σ -nitrogen atoms of the ligands bind to the metal ion and π -NH moieties form an intramolecular H-bonding network within a cavity. **Figure 3.1** shows structures of one of the urea ligands used in the past and the coordination geometry of the anion after it binds with the metal ion.

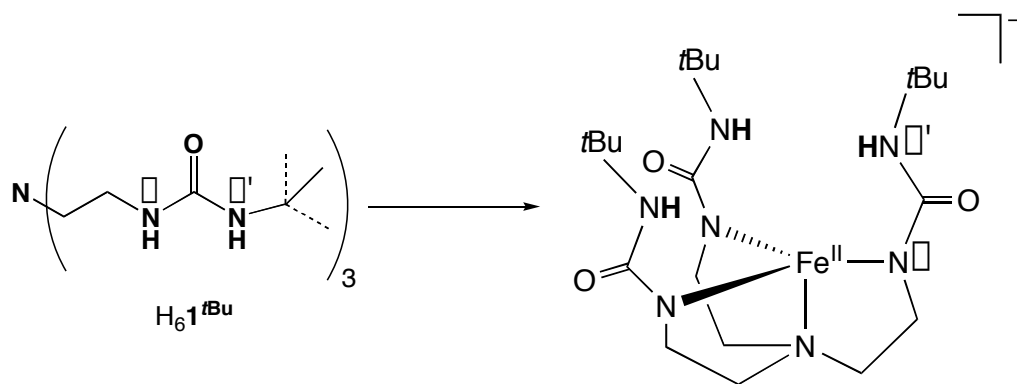


Figure 3.1. Structure of H_61^{tBu} and $[Fe^{II}H_31^{tBu}]^-$.

The anion $[Fe^{II}(H_41^{PF})_2]^{2-}$ shows tetrahedral geometry around the Fe(II) center and the primary coordination sphere around the Fe(II) center is defined by the two nitrogen atoms of $[H_41^{PF}]^{2-}$ ligand. Two ligands bind to each Fe(II) center in the crystal structure. The average Fe–N bond distance of the anion is 2.049(2) Å and the average bond angle of N–Fe–N is near 110 (°). A slight distortion from the ideal tetrahedron is observed because of the opening of N5–Fe–N46 angle to 116.93(8, °) and N45–Fe–N6 angle to 119.35(8, °); two relative shorter angles are also observed at 103.64(8, °) for N5–Fe–N6 and 102.92(8, °) for N46–Fe–N45. The bond distance and bond angle observed for a divalent Fe(II) complex, $[Fe(TC-5,5)]$ is 2.020(3) Å for the Fe– $N_{(TC)avg}$ bond and 103.4(2)° for the N–Fe–N bond angle.⁷ This iron(II) complex shows a distorted tetrahedral geometry. Typical Fe– N_{urea} distances observed for the five-coordinate Fe^{II}-complexes with tripodal urea compounds range from 2.01–2.26 Å.⁸

Analysis of the $[\text{Fe}^{\text{II}}(\text{H}_4\text{1}^{\text{PF}})_2]^{2-}$ crystal structure reveals another interesting feature. One of the urea arms of the $[\text{H}_4\text{1}^{\text{PF}}]^{2-}$ ligand does not bind to the iron center; however it forms H-bonds with the carbonyl group of another urea arm. Intramolecular H-bonds are observed between the oxygen atom of the carbonyl group (O1, O41) and the NH 's (N7, N47) and NH 's (N4, N44) of the ligand. The observed N \cdots O heavy atom distances are less than 3.0 Å, which indicate the presence of strong intramolecular H-bonds in the structure. Intramolecular H-bonds are also observed between one of the phenyl fluorine's and NH 's.

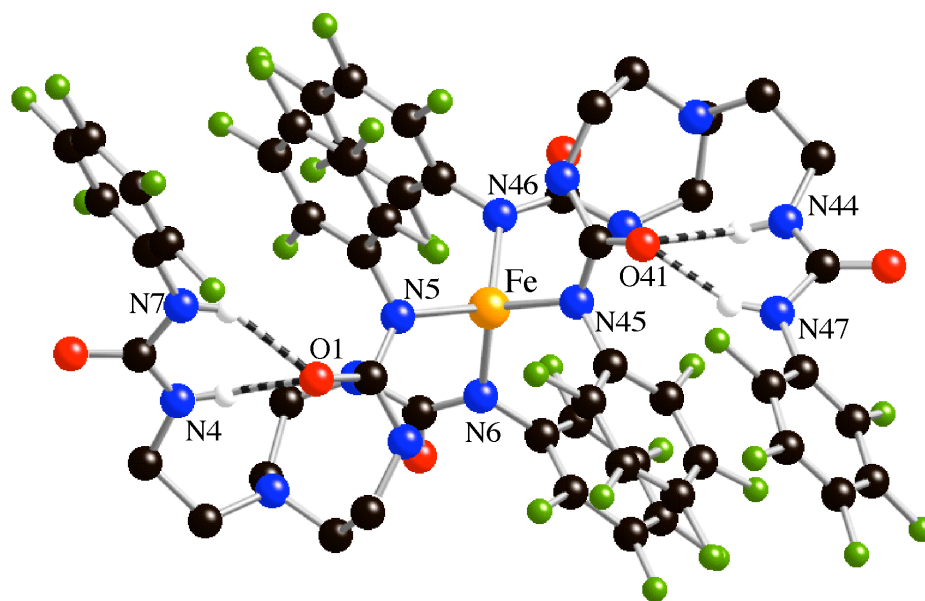


Figure 3.2. Representation of the molecular structure of $[\text{Fe}^{\text{II}}(\text{H}_4\text{1}^{\text{PF}})_2]^{2-}$.

Table 3.2 Selected bond distances (Å) and angles (°) for $\text{K}_2[\text{Fe}^{\text{II}}(\text{H}_4\text{1}^{\text{PF}})_2]$.

$\text{K}_2[\text{Fe}^{\text{II}}(\text{H}_4\text{1}^{\text{PF}})_2]$	
Fe–N5	2.059(2)
Fe–N6	2.048(2)
Fe–N45	2.052(2)
Fe–N46	2.037(2)
O1···N4	2.928(3)
O1···N7	2.828(3)
O41···N44	2.944(3)
O41···N47	2.778(3)
N5–Fe–N6	103.64(8)
N5–Fe–N46	116.93(8)
N45–Fe–N6	119.35(8)
N46–Fe–N45	102.92(8)
N45–Fe–N5	106.37(8)
N46–Fe–N6	108.34(8)

Molecular Structure Results for the Iron^{II}-Acetate Complex

Single crystal X-ray diffraction studies were performed on $\text{K}_3[\text{Fe}_2^{\text{II}}(\text{H}_3\text{1}^{\text{PF}})_2(\text{OAc})]$ crystal and the crystal, data collection and refinement parameters are given in **Table 3.3**. The asymmetric unit for crystals of $\text{K}_2(\text{O}_2\text{CCH}_3)[\{\text{Fe}(\text{C}_{27}\text{H}_{15}\text{F}_{15}\text{N}_7\text{O}_3)\}_2(\text{O}_2\text{CCH}_3)] \cdot 4\text{CH}_3\text{CON}(\text{CH}_3)_2$ grown from dimethylacetamide and ether contains one $[\{\text{Fe}(\text{C}_{27}\text{H}_{15}\text{F}_{15}\text{N}_7\text{O}_3)\}_2(\text{O}_2\text{CCH}_3)]^{2-}$ or $[\text{Fe}_2^{\text{II}}(\text{H}_3\text{1}^{\text{PF}})_2(\text{OAc})]^{2-}$ dianion, two K^+ cations and 4 dimethylacetamide molecules. The crystals have a triclinic, space group $P\bar{1}-C_1^1$ (No. 2).⁶ If the metals are Fe(II), two additional positive charges must also be present in the asymmetric unit to balance charge. Since the structure is poor and missing charges, only the connectivity among ligands and Fe(II) ions can be described. The bond length and angles are not accurate

to make definitive statements. Displacement ellipsoids are drawn at the 50% probability level. Selected bond angles and distances for the molecular structure are given in **Table 3.4**. The molecular structure of $\text{K}_3[\text{Fe}_2^{\text{II}}(\text{H}_3\text{1}^{\text{PF}})_2(\text{OAc})]$ and H-bonding interactions observed within the $\text{K}_3[\text{Fe}_2^{\text{II}}(\text{H}_3\text{1}^{\text{PF}})_2(\text{OAc})]$ complex are shown in **Figure 3.3** and **Figure 3.4**.

Table 3.3 Crystallographic parameters for $\text{K}_3[\text{Fe}_2^{\text{II}}(\text{H}_3\text{1}^{\text{PF}})_2(\text{OAc})]$.

Salt	$\text{K}_3[\text{Fe}_2^{\text{II}}(\text{H}_3\text{1}^{\text{PF}})_2(\text{OAc})]$
Empirical formula	$\text{C}_{81}\text{H}_{45}\text{F}_{45}\text{Fe}_2\text{K}_2\text{N}_{21}\text{O}_9$
Formula weight (g/mol)	2501.28
T (K)	100(2)
Space group	$P\bar{1}$
a (Å)	12.0141(7)
b (Å)	20.1639(12)
c (Å)	23.6826(14)
α (deg)	77.8030(10)
β (deg)	88.6780(10)
γ (deg)	75.0620(10)
Z	2
V (Å ³)	5415.1(6)
ρ_{calc} (Mg/m ³)	1.534
R ^a	0.2856
R _w ^b	0.6732
GOF ^c	2.746

^a $R = \frac{\sum ||F| - |F_o||}{\sum |F_o|}$. ^b $R_w = \left\{ \frac{\sum [w(F_o^2 - F_c^2)^2]}{\sum [w(F_o^2)^2]} \right\}^{1/2}$. ^cgoodness of fit on F^2 .

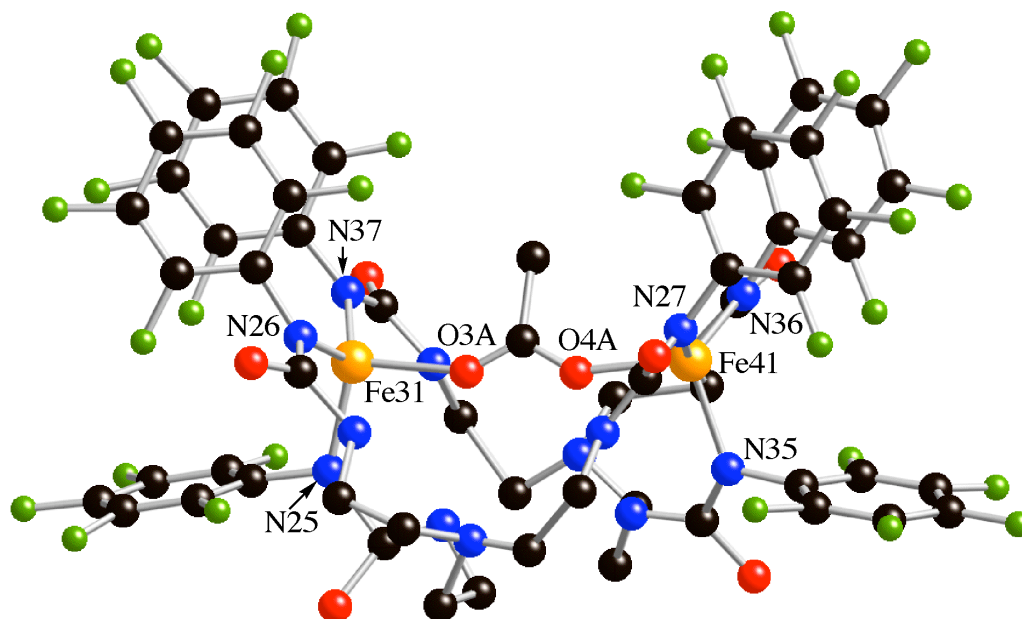


Figure 3.3. Representation of the molecular structure of $[\text{Fe}_2^{\text{II}}(\text{H}_31^{\text{PF}})_2(\text{OAc})]^{3-}$. Hydrogen atoms are omitted for clarity.

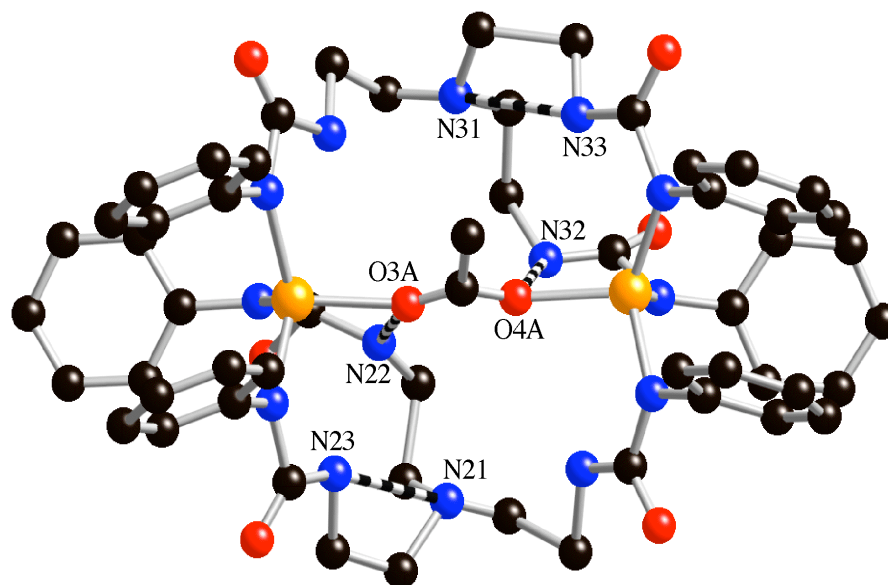


Figure 3.4. Representation of the molecular structure of $[\text{Fe}_2^{\text{II}}(\text{H}_31^{\text{PF}})_2(\text{OAc})]^{3-}$ showing intramolecular H-bonding network. Fluorine and hydrogen atoms are omitted for clarity.

Table 3.4 Selected bond distances (Å) and angles (°) for $\text{K}_3[\text{Fe}_2^{\text{II}}(\text{H}_3\text{1}^{\text{PF}})_2(\text{OAc})]$.

$\text{K}_3[\text{Fe}_2^{\text{II}}(\text{H}_3\text{1}^{\text{PF}})_2(\text{OAc})]$	
Fe31–N25	2.05(2)
Fe31–N26	1.92(3)
Fe31–N37	2.05(3)
Fe31–O3A	2.004(17)
Fe41–N35	2.00(3)
Fe41–N36	2.02(2)
Fe41–N27	2.03(2)
Fe41–O4A	2.05(2)
Fe31···Fe41	6.125(5)
N25–Fe31–N26	113.8(11)
N25–Fe31–O3A	107.3(8)
N37–Fe31–N26	110.0(11)
N37–Fe31–O3A	99.6(9)
N35–Fe41–N36	111.6(10)
N35–Fe41–O4A	102.6(8)
N27–Fe41–N36	120.8(10)
N27–Fe41–O4A	107.2(9)

The divalent diiron complex, $[\text{Fe}_2^{\text{II}}(\text{H}_3\text{1}^{\text{PF}})_2(\text{OAc})]^{3-}$ has a monobridged acetate ligand and two units of $[\text{H}_3\text{1}^{\text{PF}}]^{3-}$ ligand. The two iron subunits in the dimer are symmetric to each other and are related by a two-fold symmetry axis. The Fe(II) centers in $[\text{Fe}_2^{\text{II}}(\text{H}_3\text{1}^{\text{PF}})_2(\text{OAc})]^{3-}$ are observed to have a four coordinate-tetrahedral geometry. Each iron center in the dimer is surrounded by three of the $\square\square\text{N}$ atoms and one oxygen atom from the acetate group. Of the three $\square\square\text{N}$ atoms two of them are coming from one unit of a $[\text{H}_3\text{1}^{\text{PF}}]^{3-}$ ligand and the third $\square\square\text{N}$ comes from another $[\text{H}_3\text{1}^{\text{PF}}]^{3-}$ ligand. The molecular structure of $[\text{Fe}_2^{\text{II}}(\text{H}_3\text{1}^{\text{PF}})_2(\text{OAc})]^{3-}$ confirms that each of the pentafluorophenyl urea arms bind differently to the Fe(II) centers. For example, the urea arm containing $\square\square\text{N}27$ originates from the central amine nitrogen N21 of

one unit of $[\text{H}_3\text{1}^{\text{PF}}]^{3-}$ and it binds to one half of the dimer having the Fe41 atom; similarly, the $\square\square\text{N37}$ originates from N31 of the second unit of $[\text{H}_3\text{1}^{\text{PF}}]^{3-}$ and binds to the first half dimer having the Fe31. This binding mode avoids the steric hindrance caused by the phenyl rings and results in a rigid molecular structure. Distortions from ideal tetrahedral geometry are observed for N25–Fe31–N26 angle of 113.8(11, °) and N27–Fe41–N36 angle of 120.8(10, °). Smaller angles are found at 99.6(9, °) for N37–Fe31–O3A and 102.6(8, °) for N35–Fe41–O4A.

The metal-to-metal separation (Fe31 \cdots Fe41) for the dimer was found to be 6.125(5) Å. Bond distance observed for the Fe–O(\square -OAc) was 2.027(9) Å and the bond distances found for Fe–N bonds in each unit of the $[\text{Fe}_2^{\text{II}}(\text{H}_3\text{1}^{\text{PF}})_2(\text{OAc})]^{3-}$ dimer were close to 2.01 Å. For example, Fe31–N bond length is 2.020(3) Å and Fe41–N bond length is 1.979(2) Å. Observed Fe^{II} \cdots Fe^{II} bond distance in other acetate bridged diiron complexes are normally shorter; for instance, the Fe \cdots Fe separation in $[\text{Fe}_2(\text{OAc})_5(\text{H}_2\text{O})(\text{py})_2]^-$ and $[\text{Fe}_2(\text{O}_2\text{CR})_4(\square\text{-H}_2\text{O})(\text{tmen})_2]$ are 3.577(2) Å⁹ and 3.653(2) Å.¹⁰ These diiron complexes have two bridging acetate ligands (bis(\square -acetato)) and one aqua(\square -aqua) bridging ligand in their molecular structure. An Fe–O(\square -OAc) bond distance of 2.09(2,4) Å and an Fe–N bond distance of 2.210(6) Å and 2.222(6) Å were observed for the $[\text{Fe}_2(\text{OAc})_5(\text{H}_2\text{O})(\text{py})_2]^-$ complex.⁹ For the diiron(II) complexes, $[\text{Fe}_2(\text{O}_2\text{CMe})_2(\text{OH})(\text{Me}_3\text{TACN})_2]^-$ and $[\text{Fe}_2(\text{O}_2\text{CMe})_2(\text{O})(\text{Me}_3\text{TACN})_2]^-$ the metal-metal separation found was 3.32(1) Å and 3.12(4) Å and the Fe–O(\square -OAc) bond distance was 2.131(5) Å and 2.034(3) Å respectively.¹¹ An Fe–N bond distance of 2.29(1) Å and 2.233(5) Å was also obtained

for these complexes. Although the observed Fe–O(\square -OAc) and Fe–N bond lengths of our dimer is comparable with the other systems mentioned here, the metal-metal separation obtained for the dimer is quite different. A Fe \cdots Fe distance of 4.3598(8) Å was observed for a neutral diiron(II) complex, $[\text{Fe}_2(\square\text{-O}_2\text{CAr}^{\text{Tol}})_2(\text{O}_2\text{Ar}^{\text{Tol}})_2(\text{N},\text{N}-\text{Bn}_2\text{en})_2]$.¹² Increase in metal-metal separation on this complex was reasoned because of the steric crowding caused by the ligand *N,N*-Bn₂en. We believe that having very bulky ligands with phenyl rings in our complex could caused steric crowding in the dimer and thereby led to the increased Fe \cdots Fe bond distance of 6.125(5) Å.

The presence of intramolecular H-bonds between the oxygen atoms of the acetate group and the \square -NH's is supported by the HN22 \cdots O3A distance of 2.734 Å and N32 \cdots O4A distance of 2.834 Å. The N21 \cdots HN23 bond distance of 2.859 Å and N31 \cdots HN33 distance of 2.830 Å also supports the existence of intramolecular H-bonds between the central amine nitrogen atom and the \square -N atom.

Molecular Structure Results for the Iron^{II}-Hydroxide Complex

Single crystal X-ray diffraction studies were performed on a $\text{K}_3[\text{Fe}_3^{\text{II}}(\text{H}_3\text{1}^{\text{PF}})_2(\text{OH})_3]$ crystal and the crystal, data collection and refinement parameters are given in **Table 3.5**. Selected bond angles and distances are given in **Table 3.6**. The molecular structure and H-bonding interactions of $[\text{Fe}_3^{\text{II}}(\text{H}_3\text{1}^{\text{PF}})_2(\text{OH})_3]^{3-}$ are shown in **Figures 3.5** and **3.7**.

Table 3.5 Crystallographic parameters for $\text{K}_3[\text{Fe}_3^{\text{II}}(\text{H}_3\text{I}^{\text{PF}})_2(\text{OH})_3]$.

Salt	$\text{K}_3[\text{Fe}_3^{\text{II}}(\text{H}_3\text{I}^{\text{PF}})_2(\text{OH})_3]$
Empirical formula	$\text{C}_{89}\text{H}_{105.50}\text{F}_{30}\text{Fe}_3\text{K}_{2.62}\text{N}_{21.50}\text{Na}_{0.38}\text{O}_{18}$
Formula weight (g/mol)	2613.10
T (K)	100(2)
Space group	$P\bar{1}$
a (Å)	19.5570(7)
b (Å)	20.8428(7)
c (Å)	29.6851(10)
α (deg)	84.4750(10)
β (deg)	85.0070(10)
γ (deg)	80.6120(10)
Z	4
V (Å ³)	11851.4(7)
ρ_{calc} (Mg/m ³)	1.465
R ^a	0.1104
R _w ^b	0.3484
GOF ^c	1.071

^a $R = \frac{\sum ||F| - |F_o||}{\sum |F_o|}$. ^b $R_w = \left\{ \frac{\sum [w(F_o^2 - F_c^2)^2]}{\sum [w(F_o^2)^2]} \right\}^{1/2}$. ^cgoodness of fit on F^2 .

The crystals have a triclinic, space group $P\bar{1} - C_i^1$ (No.2).⁶ The asymmetric unit for crystals of solvated $\text{Na}_{0.39}\text{K}_{2.61}[\{\text{Fe}(\text{OH})\}_3(\text{C}_{27}\text{H}_{15}\text{F}_{15}\text{N}_7\text{O}_3)_2] \cdot 7.5\text{CH}_3\text{CON}(\text{CH}_3)_2 \cdot 0.5\text{O}(\text{C}_2\text{H}_5)_2 \cdot \text{H}_2\text{O}$ grown from dimethylacetamide and ether contains two trianions of $[\{\text{Fe}(\text{OH})\}_3(\text{C}_{27}\text{H}_{15}\text{F}_{15}\text{N}_7\text{O}_3)_2]^{3-}$ or $[\text{Fe}_3^{\text{II}}(\text{H}_3\text{I}^{\text{PF}})_2(\text{OH})_3]^{3-}$, 0.78 Na^+ and 5.22 K^+ cations. The asymmetric unit also contains a water molecule, 15 dimethylacetamide molecules and one diethyl ether solvent molecule; most of these solvent molecules are coordinated to the sodium or potassium cations and appear to be somewhat

disordered. While five of the counter ion sites seem to always be occupied by a K^+ cation, the sixth site is occupied by Na^+ 78% of the time and by K^+ 22% of the time. Six additional peaks obtained from difference Fouriers appear to belong to highly disordered solvent moieties; full-occupancy carbon atoms were included in the structural model at the sites. Displacement ellipsoids are drawn at the 50% probability level.

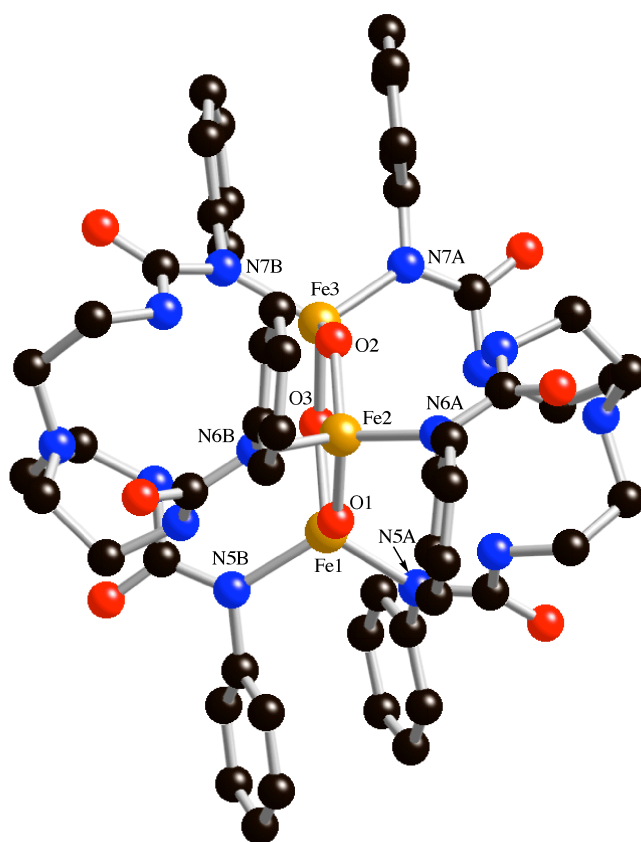


Figure 3.5. Representation of the molecular structure of $[Fe_3^{II}(H_31^{PF})_2(OH)_3]^{3-}$. Fluorine and hydrogen atoms are omitted for clarity.

The molecular structure of $[\text{Fe}_3^{\text{II}}(\text{H}_3\text{1}^{\text{PF}})_2(\text{OH})_3]^{3-}$ confirms that the Fe(II) centers are four-coordinate and have tetrahedral coordination. Each Fe(II) center in the trimer is bridged by oxygen atoms from two of the hydroxide ligands and binds with two of the $\square\square\text{N}$ atoms from each $[\text{H}_3\text{1}^{\text{PF}}]^{3-}$ ligands. The three urea arms of each ligand bind with the three Fe(II) centers on each side of the plane. The Fe and oxygen atoms, binds alternatively and form a “benzene like” structure. In addition the $(\text{Fe}-\text{OH})_3$ unit, resides within a cavity formed by the two $[\text{H}_3\text{1}^{\text{PF}}]^{3-}$ ligands. **Figure 3.6** represents the stick model of $[\text{Fe}_3^{\text{II}}(\text{H}_3\text{1}^{\text{PF}})_2(\text{OH})_3]^{3-}$, with the illustration of how the ligands bind to the $[\text{Fe}(\text{OH})_3]_3$ unit and form cavity structures.

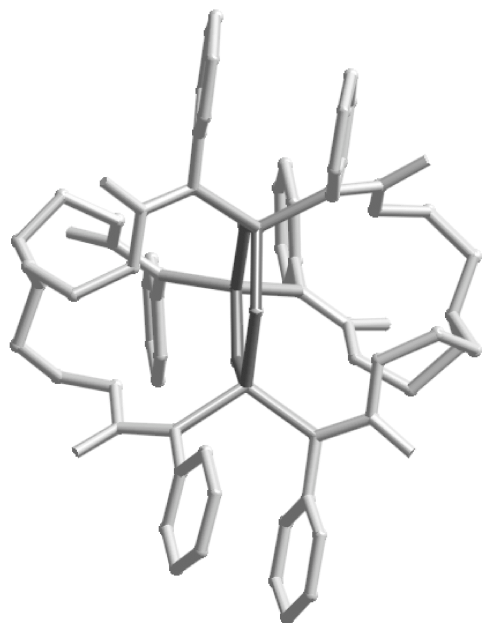


Figure 3.6. Stick model of $[\text{Fe}_3^{\text{II}}(\text{H}_3\text{1}^{\text{PF}})_2(\text{OH})_3]^{3-}$. Fluorine and hydrogen atoms are omitted for clarity.

The average bond angle in each tetrahedron is $110.9(4, ^\circ)$ and the $\text{Fe}-\square-\text{O}-\text{Fe}$ bond angle is $134.3_{\text{avg}}(4, ^\circ)$. Each tetrahedron has a Fe–N bond distance of $2.035(8) \text{ \AA}$ and Fe–O distance of $2.001(7) \text{ \AA}$. The Fe–OH bond distance observed for a monomeric

Fe^{II} -terminal hydroxo trigonal bipyramidal complex is 2.051(3) Å and 2.044(3) Å^{8b} and for a mononuclear tetrahedral Fe^{II} -OH complex is 1.830(8) Å.¹³ The dinuclear square pyramidal bis- μ -hydroxo bridged dimeric Fe^{II} -OH complex, $[\text{Fe}(\text{HB}(3,5\text{-iPr}_2\text{pz})_3)]_2-(\mu\text{-OH})_2$ shows an Fe-OH bond distance of 2.016(9) Å and 2.04(1) Å.¹⁴ To the best of our knowledge this is the first example of a trinuclear Fe^{II} -OH complex isolated with a hexagon core of (Fe-OH)₃ unit. The closest example is a hexagon (Fe-O)₃ core observed for a Fe^{III} -oxo complex with ligand 5-Et₃-TPA [tris(5-ethyl-2-pyridylmethyl)amine].¹⁵ The Fe- μ -O bond distance of 1.84_{avg} Å and Fe- μ -O-Fe bond angle of 132.9_{avg} (°) is observed for this complex. The observed Fe- μ -O-Fe bond angles are comparable with the trimer $[\text{Fe}_3^{\text{II}}(\text{H}_3\text{l}^{\text{PF}})_2(\text{OH})_3]^{3-}$.

A total number of six intramolecular H-bonds are observed between the μ -NH's and the oxygen atoms of the hydroxide ligands and the H-bond distance observed between N \cdots O heavy atoms is 3.062 Å. The μ -NH groups also hydrogen bond with the apical nitrogen atoms: observed bond distances of 2.982 Å for N1B \cdots HN3B, 2.935 Å for N1A \cdots HN3A and 2.992 Å for N1A \cdots HN4A support the presence of intramolecular H-bonds in the trimer.

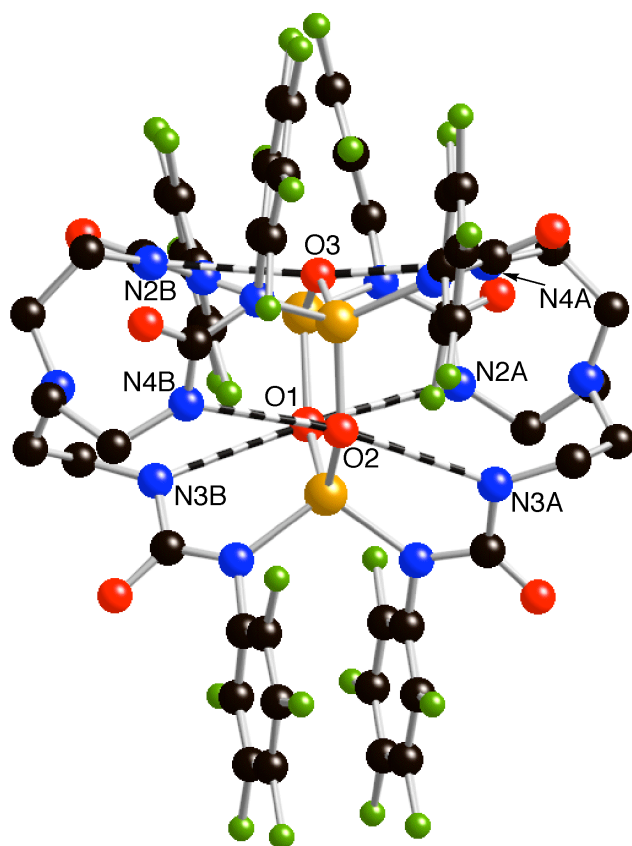


Figure 3.7. H-bonding network of $[\text{Fe}_3^{\text{II}}(\text{H}_3\text{l}^{\text{PF}})_2(\text{OH})_3]^{3-}$. Hydrogen atoms are omitted for clarity.

Table 3.6 Selected bond distances (Å) and angles (°) for $\text{K}_3[\text{Fe}_3^{\text{II}}(\text{H}_3\text{I}^{\text{PF}})_2(\text{OH})_3]$.

$\text{K}_3[\text{Fe}_3^{\text{II}}(\text{H}_3\text{I}^{\text{PF}})_2(\text{OH})_3]$	
Fe1–N5A	2.021(9)
Fe1–N5B	2.049(8)
Fe1–O1	2.010(6)
Fe1–O3	1.993(7)
Fe2–N6A	2.031(8)
Fe2–N6B	2.028(8)
Fe2–O2	2.012(7)
Fe2–O1	1.995(7)
Fe3–N7A	2.017(9)
Fe3–N7B	2.026(10)
Fe3–O3	1.998(7)
Fe3–O2	1.984(7)
N2A···O1	3.004(10)
N3A···O2	3.075(10)
N4A···O3	3.068(10)
N2B···O3	3.109(10)
N3B···O1	3.035(10)
N4B···O2	3.079(11)
Fe1–O1–Fe2	135.9(4)
Fe2–O2–Fe3	132.9(4)
Fe3–O3–Fe1	134.2(3)
N5B–Fe1–N5A	107.2(4)
N5A–Fe1–O3	113.3(3)
O3–Fe1–O1	104.3(3)
O1–Fe1–N5B	113.8(3)
O1–Fe1–N5A	108.6(3)
O3–Fe1–N5B	109.7(3)
N6B–Fe2–N6A	107.5(3)
N6A–Fe2–O2	109.7(3)
O2–Fe2–O1	105.3(3)
O1–Fe2–N6B	108.0(3)
O1–Fe2–N6A	112.6(3)
O2–Fe2–N6B	113.9(3)
N7B–Fe3–N7A	110.3(4)
N7A–Fe3–O3	106.1(3)
O3–Fe3–O2	107.4(3)
O2–Fe3–N7B	107.2(4)
O2–Fe3–N7A	113.6(3)
O3–Fe3–N7B	112.4(4)

Stacking Arrangements in Phenyl Rings

Noncovalent aromatic-aromatic interactions of aromatic rings give rise to several possibilities of π -stacking orientations; they are the off-centered parallel-displaced, T-shaped stacking, parallel-staggered and the herringbone orientations.¹⁶⁻¹⁹ Of these interactions proteins and DNA/RNA bases most commonly show the off-centered parallel-displaced stacking. **Figure 3.1** represents schematic representations of all four possible π -stacking geometries.

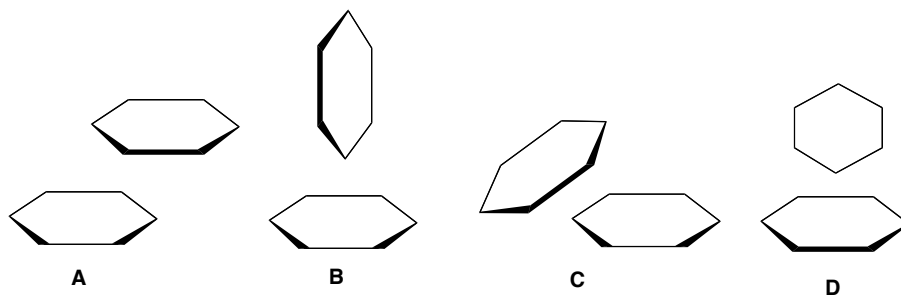


Figure 3.8. Commonly observed aromatic-aromatic interactions (A) off-centered parallel-displaced orientation (B) T-shaped orientation (C) parallel-staggered orientation (D) herringbone orientation.

Molecular structures obtained for all three Fe^{II} -complexes (monomer, dimer, and trimer) show either off-centered parallel-displaced, or T-shaped π -stacking geometries between pentafluorophenyl rings. Both the monomer and the trimer shows only the off-centered parallel-displaced stacking geometry between phenyl rings: however the dimer, $[\text{Fe}_2^{\text{II}}(\text{H}_3\text{1}^{\text{PF}})_2(\text{OAc})]^{3-}$ itself shows both off-centered parallel displaced, and T-shaped π -stacking orientations. One of the phenyl rings orients itself

in a slightly distorted T-shaped stacking geometry to the other two parallel-displaced phenyl rings.

Conclusion

Three different metal complexes were prepared when the ligand H_61^{PF} was treated with different equivalents of base and metal precursor. Addition of two equivalents of base and half-equivalent of iron acetate produces a monomeric metal complex, which shows strong intramolecular H-bonding interactions between the carbonyl oxygen atom and the urea nitrogens. A dimeric metal complex was produced with three equivalents of base and one equivalent of iron acetate. The two iron atoms are bridged through an acetate group. Intramolecular H-bonding interactions were observed, and a very long metal-metal distance was also observed for this complex.

The third complex was a trimer and was isolated when four equivalents of base, one equivalents of iron acetate and one equivalents of water were added to the ligand in a DMA solution. This Fe^{II} -hydroxide complex has a unique structure: the alternating Fe and oxygen atoms forms a hexagonal arrangement inside a cavity formed by the two $[H_31^{PF}]^{3-}$ ligands. Similar primary coordination spheres were observed around the iron centers in all the three complexes. They showed tetrahedral geometry around the Fe^{II} center with nitrogen donors from two different $[H_31^{PF}]^{3-}$ ligands. The complexes show two different π -stacking orientations between the pentafluorophenyl rings. An off-centered parallel displaced, and T-shaped π -stacking

geometry is observed for the phenyl rings of the dimer and only an off-centered parallel-displaced geometry is observed for both the monomer and the trimer.

References

1. X-ray diffraction analysis was conducted by Victor Day.
2. Data Collection: *SMART Software Reference Manual*; Bruker-AXS: Madison, WI, 1998.
3. Data Reduction: *SAINTE Software Reference Manual*; Bruker-AXS: Madison, WI, 1998.
4. Sheldrick, G. M. *SADABS: Program for Empirical Absorption Correction of Area Detector Data*; University of Göttingen: Germany, 2002.
5. Sheldrick, G. M. *SHELXTL Version 6.10 Reference Manual*; Bruker-AXS: Madison, WI, 2000.
6. *International Tables for Crystallography*; Kluwer Academic Publishers: Boston 1996: Vol A.
7. Franz, K. J.; Lippard, S. J. NO Disproportionation Reactivity of Fe Tropocoronand Complexes. *J. Am. Chem. Soc.* **1999**, *121*, 10504-10512.
8. (a) Zart, M. K.; Sorrell, T. N.; Powell, D.; Borovik, A. S. Development of Bio-Inspired Chelates with hydrogen Bond Donors: Synthesis and Structure of Monomeric Metal Acetate Complexes with Intramolecular Hydrogen bonds. *Dalton Trans.* **2003**, *10*, 1986-1992. (b) MacBeth, C. E.; Hammes, B. S.; Young, Jr., V. G.; Borovik, A. S. Hydrogen Bonding Cavities about Metal Ions: Synthesis, Structure, and Physical Properties for a Series of Monomeric M-OH Complexes Derived from Water. *Inorg. Chem.* **2001**, *40*, 4733-4741.
9. Coucouvanis, D.; Reynolds III, R. A.; Dunham, W. R. Synthesis and

- Characterization of a New Class of Asymmetric Aqua-Acetate Bridged Dimers. Solid State Molecular Structures of the $[M_2(\square-H_2O)(\square-OAc)_2(OAc)_3(py)_2]^-$ Anions (M= Mn(II), Fe(II), Co(II)). A Structural Model for the Fe₂ Site in Methane Monooxygenase. *J. Am. Chem. Soc.* **1995**, *117*, 7570-7571.
10. Hagen, K. S.; Lachicotte, R. Diiron(II) \square -aqua bis(\square -carboxylato) Models of Reduced Dinuclear Non-Heme Iron Sites in Proteins. *J. Am. Chem. Soc.* **1992**, *114*, 8741-8742.
11. Hartman, J. R.; Rardin, R. L.; Chaudhuri, P.; Pohl, K.; Wieghardt, K.; Nuber, B.; Weiss, J.; Papaefthymiou, G. C.; Frankel, R. B.; Lippard, S. J. Synthesis and Characterization of (\square -hydroxo)bis(\square -acetato)diiron(II) and (\square -oxo)bis(\square -acetato)diiron(III) 1,4,7-Trimethyl-1,4,7-triazacyclononane Complexes as Models for Binuclear Iron Centers in Biology; Properties of the Mixed Valence Diiron(II,III) Species. *J. Am. Chem. Soc.* **1987**, *109*, 7387-7396.
12. Lee, D.; Lippard, S. J. Oxidative N-Dealkylation of a Carboxylate-Bridged Diiron(II) Precursor Complex by Reaction with O₂ Affords the Elusive $\{Fe_2(\square-OH)_2(\square-O_2CR)\}^{3+}$ Core of Soluble Methane Monooxygenase Hydroxylase. *J. Am. Chem. Soc.* **2001**, *123*, 4611-4612.
13. Hikichi, S.; Ogihara, T.; Fujisawa, K.; Kitajima, N.; Akita, M.; Moro-oka, Y. Synthesis and Characterization of the Benzoylformate Ferrous Complexes with the Hindered Tris(pyrazolyl)borate Ligand as a Structural Model for Mononuclear Non-Heme Iron Enzymes. *Inorg. Chem.* **1997**, *36*, 4539-4547.

14. Kitajima, N.; Tamura, N.; Tanaka, M.; Moro-oka, Y. Synthesis and Molecular Structures of Diferrous Complexes Containing a Bis(hydroxo) or a Hydroxo Carboxylato Bridge. *Inorg. Chem.* **1992**, *31*, 3342-3343.
15. Zheng, H.; Zang, Y.; Dong, Y.; Young, Jr., V. G.; Que, Jr., L. Complexes with $\text{Fe}^{\text{III}}_2(\text{L}-\text{O})(\text{L}-\text{OH})$, $\text{Fe}^{\text{III}}_2(\text{L}-\text{O})_2$, and $[\text{Fe}^{\text{III}}_3(\text{L}_2-\text{O})_3]$ Cores: Structures, Spectroscopy, and Core Interconversions. *J. Am. Chem. Soc.* **1999**, *121*, 2226-2235.
16. Mignon, P.; Loverix, S.; Steyaert, J.; Geerlings, P. Influence of the $\pi-\pi$ Interaction on the Hydrogen Bonding Capacity of Stacked DNA/RNA Bases. *Nucleic Acids Research*, **2005**, *33*, 1779-1789.
17. Gazit, E. A Possible Role for π -Stacking in the Self-Assembly of Amyloid Fibrils. *The FASEB journal*. **2002**, *16*, 77-83.
18. McGaughey, G. B.; Gagné[§], M.; Rappé[¶], A. K. π -Stacking Interactions: ALIVE AND WELL IN PROTEINS. *J. Biol. Chem.* **1998**, *273*, 15458-15463.
19. Sun, S.; Bernstein, E. R. (1996) Aromatic van der Waals Clusters: Structure and Nonrigidity. *J. Phys. Chem.* **1996**, *100*, 13348-13366.